Exploring the material composition of Hellenistic painted stucco in the southern Coastal Plain of Palestine: insights from Ashdod-Yam, Yavneh-Yam, and Tel Ya'oz

Dana Ashkenazi[*, a], Alexander Fantalkin[b], David E. Friesem[c], Yael Kochin[c], Oren Tal[b]

[a] Tel Aviv University, Israel
[b] Department of Archaeology and Ancient Near Eastern Cultures, and Institute of Archaeology, Tel Aviv University, Israel
[c] School of Archaeology and Maritime Cultures, and Recanati Institute of Maritime Studies Faculty of Humanities, University of Haifa, Israel
***** Corresponding author's email address: danaa@tauex.tau.ac.il

Keywords

Hellenistic stucco; natural pigment; plaster; southern Coastal Plain, Israel; Philistia; Ashdod-Yam; Tel Ya'oz; Yavneh-Yam

Abstract

Fragments of painted plaster (stucco) recovered from walls of buildings attributed to the Hellenistic (Seleucid) strata at the sites of Ashdod-Yam, Yavneh-Yam, and Tel Ya'oz (Israel) were subjected to different analyses in order to gain information on the composition, microstructure, production methods, and origin of both their plaster and color pigments. Macroscopic examination, together with SEM-EDS, FTIR, and XRD analyses, has been employed for this purpose. Wall plaster from all sampled fragments was found to be made of a calcite binder mixed with different aggregates, including quartz sand, crushed shells, and ceramic inclusions. Compositional and microstructural analyses indicate that pigments were mixed with fine plaster powder. Plaster, mortar, and pigments of the analyzed stucco fragments were likely locally sourced, contributing to our understanding of regional practices in the southern Levant during the Seleucid period.

1. Introduction

Excavations of Hellenistic and Roman sites in the southern Levant have revealed substantial quantities of stucco fragments, indicating that fine stucco was frequently used for decorating interior walls, while coarser stucco was applied to imitate architectural elements (Rozenberg, 2008: 298–424). Although many stucco remains remain unpublished, current evidence suggests that during the Hellenistic period, particularly in the 2nd century BCE, a distinct common language of stucco ornamentation developed and became a characteristic feature of both private and public structures (Rozenberg, 2019). This article explores the material composition of Hellenistic painted stucco in the southern Coastal Plain of Palestine, focusing on the sites of Ashdod-Yam, Yavneh-Yam, and Tel Ya'oz. The objective of this study is to determine whether this region reflects a shared expertise of stucco production and decoration during the Hellenistic period or whether it was characterized by multiple, diverse production workshops.

1.1 Archaeological background

Ashdod-Yam (Azotos Paralios) is situated on the southern coast of Israel (Fig. 1), within the confines of the modern city of Ashdod. Archaeological excavations have uncovered the remains of a monumental fortress that dates to the Hellenistic period (Stratum II) (Ashkenazi and Fantalkin, 2019; Fantalkin et al., 2024). The surviving foundations of the fortress walls were constructed of well-dressed *kurkar* (fossilized dune sandstone) blocks incorporating finely dressed limestone monoliths. Adjacent auxiliary structures built of mudbricks atop stone foundations of partially hewn local beachrock (Area A) accompanied the fortress. These structures likely constituted part of a defensive fortification line encircling the entire military complex. This included a mudbrick wall integrated with watchtowers constructed from partially hewn beachrock and mudbricks.

The stucco fragments analyzed in this study derive from the fortress (Area A1), the auxiliary structures (Area A), and one of the watchtowers (Area D East). A plan of the excavated remains at Ashdod-Yam, showing the locations of the examined stucco fragments, is presented in Appendix A (Fig. A1).

Based on numismatic and ceramic evidence, the fortress with its associated auxiliary structures were established during the first half of the 2nd century BCE, within the context of Seleucid military activities. Although it remains difficult to determine under which Seleucid king this military stronghold was initially commissioned, it was likely reinforced during the tenure of

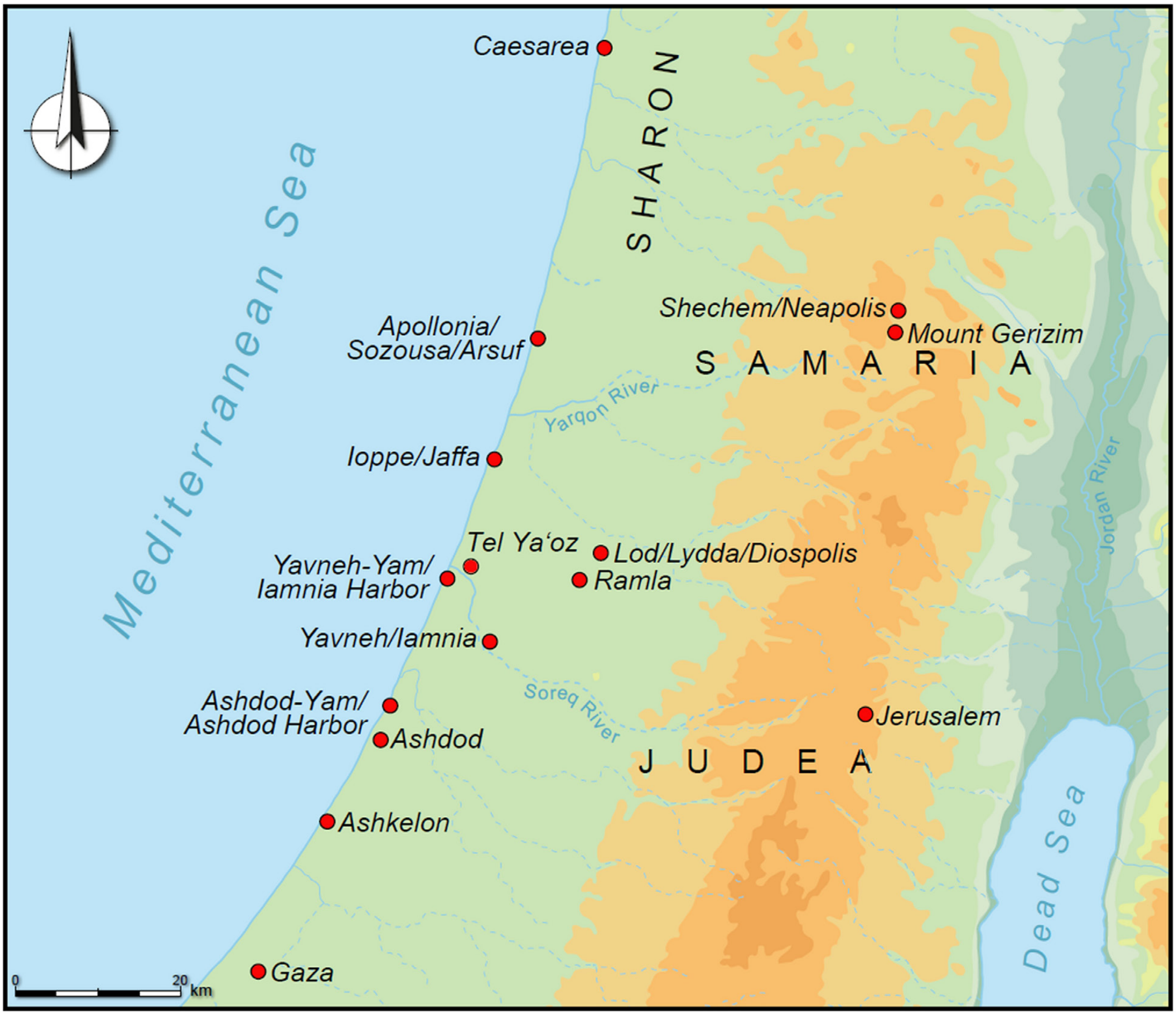

Figure 1. Map showing the location of the sites discussed (Tel Ya'oz, Ashdod-Yam, Yavneh-Yam) and neighboring sites.

Antiochus VII Sidetes under his general Cendebaeus, and subsequently destroyed by John Hyrcanus I toward the end of his reign, in the late 2nd century BCE, contemporaneously with the destruction of Tel Ashdod Phase 3b (Fantalkin et al., 2024).

Yavneh-Yam (Iamnia Paralios) lies south of Kibbutz Palmaḥim on the Mediterranean shoreline (Fig. 1), approximately equidistant (20 km apart) from Ioppe/Jaffa and Azotos Paralios/Ashdod-Yam. General Cendebaeus, appointed by Antiochus VII Sidetes as the commander of the Palestinian coast, established Iamnia Paralios as his operational base, from which he launched military campaigns against Judea. Remains from the Hellenistic period (Stratum VI) were unearthed at Yavneh-Yam mainly in Area A (Fischer, 2008), where a building had been erected over the ruins of an earlier Persian-period structure, reusing some of its walls and building materials. A plan of the excavated Hellenistic remains in Area A, showing the locations of the examined stucco fragments, is presented in Appendix A (Fig. A2).

Some of the Hellenistic-period building stones were partly covered with painted stucco, analyzed here. Finds from the Hellenistic stratum, including numismatic evidence, strongly indicate that occupation continued until the late 2nd century BCE, culminating in significant destruction (Fischer et al., 2023). The destruction of Yavneh-Yam Stratum VI appears to coincide with the destruction of Ashdod-Yam Stratum II, most likely attributable to the military campaigns of John Hyrcanus I near the end of his reign or the beginning of that of Alexander Jannaeus (Fantalkin et al., 2024).

Tel Yaʻoz (Gazara/Tell Ghazza) is located on the southern border of the Rishon LeZion dunes, about 1 km north of the bend in Naḥal Soreq (Wadi Rubin), and roughly 1.5 km east of the Mediterranean shoreline (Fig. 1). The stucco fragments illustrated in the site's excavation report (Fischer et al., 2008: 141, fig. 23 [Item 6]) and analyzed here originated in various loci in Area A. Some fragments belong to attachments between pilasters and the wall (A1) to which they were affixed, which the excavators reconstructed as possibly belonging to a monumental Hellenistic-Seleucid building (Fischer et al., 2008: 145–146). Wall A1 was built mainly of dressed *kurkar* slabs, with a *ḥamra*-based mortar. Its upper courses consist of alternating headers and stretchers that formed the foundation for a brick wall once covered by the stucco fragments (Fischer et al., 2008). A plan of the excavated remains in Area A, showing the location of the examined stucco fragment, is provided in Appendix A (Fig. A3).

1.2 Technological background: plaster, mortar, and pigments

Plaster and mortar are fundamental building materials used throughout human history for both structural and decorative purposes. These materials are composed of an inorganic binder, most commonly lime, mixed with aggregates and water to form a paste that hardens over time (Bochen and Labus, 2013; Vázquez de Ágredos-Pascual et al., 2019; Ali and Youssef, 2020; Ali and Elrahim, 2021; Arizzi and Cultrone, 2021). Although their compositions are similar, their functions differ: mortar was used primarily as a binding material for joining stones and/or bricks, whereas plaster was applied as a smooth finishing layer for coating and decoration. Typically, mortars are coarser and thicker, while plasters are finer and smoother in texture (Ashkenazi et al., 2021).

Lime-based plasters and mortars typically consist of calcium carbonate (calcite, $CaCO_3$) and hydrated (slaked) lime [calcium hydroxide, $Ca(OH)_2$], combined with various aggregates such as quartz/silica sand (composed primarily of SiO_2), crushed stones, and/or gypsum (Ali and Youssef, 2020; Ali and Elrahim, 2021; Arizzi and Cultrone, 2021). Gypsum powder ($CaSO_4 \cdot ½H_2O$) is produced by heating natural gypsum ($CaSO_4 \cdot 2H_2O$) to 120–180 °C, releasing water as steam. Hydrated lime is formed when water is added to lime (CaO) in an exothermic reaction, completing the lime cycle—calcination, slaking, and carbonation (Ergenç et al., 2021; Medeghini et al., 2024). The production of lime plaster required considerable technological expertise and is first attested in the Late Epipalaeolithic Natufian culture (at least 12,000 years BP) in the Levant, where lime plaster was used in both architectural and mortuary contexts (Kingery et al., 1988; Friesem et al., 2019; Friesem et al., 2020). Non-pyrogenic calcite-based plasters were also in use during this period (Friesem et al., 2020). Lime- and gypsum-based materials became widespread across the Middle East during the 7th and 8th millennia BCE (Kingery et al., 1988; Ergenç et al., 2021), often containing mineral inclusions such as quartz, potassium feldspars, and hematite (α-Fe_2O_3) (Klempan et al., 2017).

Both plasters and mortars can be either aerial/pure lime (non-hydraulic) or hydraulic, depending on the binder. Hydraulic plasters and mortars are produced by mixing slaked lime with highly disordered silicate minerals. While aerial lime binders are composed of pure carbonate, with less than 5% silicates, hydraulic lime binders contain either pure carbonate or impure carbonate mixed with clays (Ergenç et al., 2021). There are also non-pyrogenic (non-lime) plasters. For example, the walls, ceilings, and fine-grained floors of the Middle Bronze Age Canaanite palace complex at Tel Kabri were made of lime plaster, whereas the thick, coarse floors at the site were composed of pulverized chalk (non-pyrogenic plaster; Goshen et al., 2017). Similar features are evident elsewhere. For example, at the Iron Age IIA settlement of Kh. es-Suwweida, two main building technologies were identified: the production of lime plasters from mixtures of pyrogenic lime and non-pyrogenic (geogenic) crushed chalk, and the manufacture of mudbricks from sedimentary materials (Grono et al., 2024). Pizzo et al. (2024) assert that workers in both Hellenistic and Roman contexts effectively utilized local raw materials, demonstrating a high degree of expertise in enhancing the performance of mortar and plaster mixtures and producing durable, resilient materials.

Earth pigments are inorganic, naturally occurring mineral pigments used as colorants. They can be divided into two main categories: (1) non-clay pigments and (2) pigments in which the chromophore element is embedded in the crystal structure of the clay material, absorbing light at a specific wavelength (Sharma and Singh, 2021). Pedogenic hematite from red terra rossa soils was the main reddening agent in the Mediterranean during antiquity (Sandler et al., 2023). The term "ochre" refers to natural earth pigments composed of metal oxides or oxide hydroxides derived from rocks, with color determined by the non-clay component (Ashkenazi et al., 2021; Sharma and Singh, 2021). Iron (Fe)-rich ochres are the most common, yet copper (Cu) and cobalt ochres were occasionally used as well. Ochre pigments are mixed with different quantities of other materials, such as sand and clay. Ochre colors vary and include yellow, umber, red, sienna, brown, and purple, depending on pigment composition (Sharma and Singh, 2021).

The color of ochre depends on three main factors: (1) the presence of Fe-oxide chromophore, with red ochres containing hematite and paler yellow ochres containing goethite [α-FeO(OH) or $Fe_2O_3{\cdot}H_2O$]; (2) the existence of secondary coloring ingredients, including other metal oxides or clay minerals; and (3) pigment particle size distribution and density (Ashkenazi et al., 2021; Sharma and Singh, 2021; Asscher et al., 2025).

During the Hellenistic and Roman periods, various pigments were used for decorative purposes, including ochre pigments, applied in wall paintings of public places, fortresses, houses, and tombs (Amadori et al., 2015; Guirdzhiiska et al., 2017; Marketou et al., 2019; Radpour et al., 2019; Ashkenazi et al., 2021; Mastrotheodoros and Beltsios, 2022). While the choice of specific colors or pigments may reflect personal or communal aesthetic preferences, which differ between periods, it may also result from geographical limitations, regional availability of raw materials, or economic considerations (Apostolaki et al., 2006; Radpour et al., 2019; Ashkenazi et al., 2021).

Characterizing plaster and pigments provides important archaeological and technological insights into local material culture, including production practices, intercommunal knowledge-sharing, wall-painting techniques, and the available palette of pigments in the region during the relevant period, as well as trends and regional and long-distance trade relations (Amadori et al., 2021; Ashkenazi et al., 2021; Dayet, 2021; Bonnie et al., 2025).

The most common analytical methods used for identifying plasters, mortars, and pigments include scanning electron microscope with energy-dispersive spectroscopy (SEM-EDS), X-ray fluorescence (XRF), X-ray diffraction (XRD), Raman spectroscopy, and Fourier-transform infrared (FTIR) spectroscopy (Mateos et al., 2018; Ravi et al., 2018; Marketou et al., 2019; Singh et al., 2019; Moropoulou et al., 2000; Guglielmi et al., 2020; Amadori et al., 2021; Ashkenazi et al., 2021; Mastrotheodoros and Beltsios, 2022; Cortea et al., 2024). Additional methods include neutron activation analysis (NAA), particle-induced X-ray emission (PIXE), inductively coupled mass spectrometry (ICP-MS), and X-ray photoelectron spectroscopy (XPS) (Sharma and Singh, 2021).

SEM-EDS provides elemental analysis using an EDS detector and identifies mineral phases on the sample's surface through back-scattered electron (BSE) imaging, which reveals chemical contrasts that can be correlated with the compositional data. According to Dayet (2021), SEM-EDS is the most recommended method for pigment characterization. However, multiple analytical methods should be used when possible to reduce the risk of misinterpretation. Recommended methods for elemental analysis of plaster, mortar, and pigment are SEM-EDS, PIXE, XRF, NAA, and ICP-MS. Recommended techniques for mineralogical characterization of plasters, mortars, and pigments include XRD, Raman spectroscopy, and FTIR, supplemented by thermogravimetric analysis (TGA) or Mössbauer spectroscopy (Ashkenazi et al., 2021; Dayet 2021; Singh et al., 2019).

The central research question of this study is how plaster, mortar, and color pigments were produced and applied in Hellenistic wall paintings at Ashdod-Yam, Yavneh-Yam, and Tel Ya‘oz, and to what extent these materials and techniques reflect a distinct local know-how of stucco decoration versus the influence of multiple production workshops in the region. To address this question, we characterize the plaster and color pigments from Hellenistic-period wall paintings at the three sites. We employ chemical composition and microstructural analyses, complemented by archaeological and geographical data, to enhance our understanding of pigment origins and the technologies used in the production of plaster, mortar, and paint. Our goal is to illuminate manufacturing techniques and the use of plaster, mortar, and natural earth pigments in Hellenistic Palestine and to determine whether the region reflects a distinct local expertise of stucco decoration or a diversity of production workshops.

2. Research methodology

To address the research objectives, a comprehensive methodology was implemented, consisting of the following steps:

(1) conducting a thorough literature review to provide background on the Hellenistic strata of the three studied sites, as well as on plaster, mortar, pigments, and common analytical methods used to identify these materials;
(2) formulating the research questions and objectives;
(3) detailing the experimental and analytical methods employed for the characterization of the stucco fragments, combining VT, SEM-EDS, FTIR, and XRD analyses;
(4) presenting the results of the material analyses;
(5) interpreting and discussing the findings within their archaeological and technological contexts.

2.1 Experimental methods

Materials characterization was carried out on fragments of painted plaster (stucco) from Hellenistic walls at Ashdod-Yam (Samples AY1–AY7), Yavneh-Yam (Samples YY1–YY3) and Tel Ya‘oz (Samples TY2.1, TY2.2, TY3, TY4, TY5.1–TY5.5, TY6.1–TY6.5). Details of these fragments are presented in Appendix B, Table B1. The samples were examined using the following methods:

2.1.1 Visual testing (VT)

VT of the painted plaster fragments was performed to detect visible characteristics such as pigment tones, surface texture, presence of inclusions or aggregates and cracks, and signs of deterioration. These observations aided in assessing preservation conditions and identifying features relevant to manufacturing processes of the plaster and paint.

To document and characterize the pigments applied to the wall plasters, a macroscopic investigation was carried out using a Canon R6II camera equipped with an extension macro ring. Each fragment was photographed in natural daylight, capturing both the planar surface (PS) and the transverse cross-section (TCS). The high-resolution images enabled the creation of a color reference catalogue that served as a visual database for comparing pigment tones and correlating observed hues with published data. This macroscopic documentation provided a consistent visual framework for describing the chromatic variability of the examined stucco fragments.

2.1.2 SEM-EDS analysis

SEM imaging combined with EDS chemical analysis was performed using an environmental SEM (ESEM). Examination was carried out in low vacuum mode. Carbon adhesive tape was applied around the samples to ensure proper electrical conductivity. The plaster fragments were characterized using an FEI Quanta 200 FEG ESEM instrument equipped with an Everhart–Thornley secondary electron (SE) detector; both SE and backscattered electron (BSE) modes were applied. EDS analysis was carried out with a Si(Li) liquid-cooled Oxford X-ray detector calibrated using standard manufacturer-provided reference materials.

2.1.3 FTIR spectroscopy

Mineralogical analysis was carried out using FTIR spectroscopy to identify mineral phases in the plaster fragments and infer technological aspects of production. A selected set of samples (n = 11: AY2, AY5–AY7, YY1–YY3, and TY1–TY4; Appendix B, Table B1) was subdivided in the lab (n = 29, Table 1) to enable identification of multiple components within each sample. Spectra were collected with a Nicolet iS5 FTIR spectrometer (Thermo Scientific) in transmission mode using the KBr method, covering a range of 4000 to 400 cm^{-1}, with a 4 cm^{-1} resolution. Results were interpreted using the Kimmel Center for Archaeological Science Infrared Standards Library (Weizmann Institute of Science).

Clay mineral alteration was evaluated to determine whether raw materials in the plaster had been exposed to high temperatures (> 500 °C), either intentionally during preparation or accidentally through fire. This was assessed on the basis of the presence (unaltered) or absence (altered) of absorption bands at 3695, 3625, and 915 cm^{-1} (Berna et al., 2007). To evaluate the degree of atomic order/disorder in calcite, associated with its formation mechanisms (e.g., geological or pyrogenic), the v2 and v4 absorption bands at 874 and 713 cm^{-1}, respectively, were studied. Changes in their height were recorded through repetitive grinding of samples (n = 30) in which calcite is a major component, following Regev et al. (2010). Determining the degree of atomic order in calcite assists in distinguishing between naturally occurring (geological) calcite and calcite formed through thermal decomposition of limestone followed by re-carbonation—typical of lime-based plasters and mortars. This distinction provides insights into the raw materials and technological processes of plaster and mortar production (Regev et al., 2010). In all, 201 spectra were generated for this study.

2.1.4 XRD analysis

XRD analysis was performed to identify the crystalline phases of the red paint. The XRD pattern was obtained using a Bruker D8 Discover Diffractometer used in a theta–theta (Θ:Θ) geometry, with Göbel Mirror to produce a parallel beam, coupled with longitudinal Soller slits to focus on the surface of the sample. The source was a sealed X-ray tube with a copper anode operating at 40 kV tube voltage and 40 mA tube current. Diffraction patterns were collected using a LYNXEYE XE linear detector in the 20–70 (2Θ) range, with a step size of 0.04° (2Θ) for 1 second per step.

3. Results

3.1 The stucco fragments from Ashdod-Yam (AY)

VT (Fig. 2) and macroscopic observation (photographic catalogue, Fig. 3) were conducted to examine the stucco fragments from Ashdod-Yam. A general description and comparison of the samples are presented here. The examined fragments share several characteristics, including the application of similar red pigment over a bright plaster base and the presence of mineral and shell inclusions. However, variations were observed in pigment tones—including the presence of black pigment in Sample AY5—as well as in layering structures and surface preservation. These variations may reflect differences in wall function and decorative design, as well as variable exposure to environmental and post-depositional conditions, rather than distinct production technologies. The repeated occurrence of quartz particles and marine shells in several samples suggests the use of coastal sand in the preparation of the plaster and mortar materials (Pizzo et al., 2024). A concise summary of the macroscopic and visual observations for each AY sample, including pigment color, layering, and visible inclusions, is presented in Table 1.

SEM observations of the red-painted surfaces of the Ashdod-Yam samples reveal compositional and textural differences between the pigment layers and the surrounding plaster. On the red-painted surface of Sample AY4 (Fig. 4a–b), the pigment layer appears brighter than the surrounding plaster in BSE imaging (Fig. 4c). This brightness reflects the higher content of heavy elements, primarily Fe in the form of Fe oxide (Fe_2O_3), which is heavier than the calcium (Ca) and silicon (Si) oxides in the plaster matrix. As a result, Fe-rich pigment particles appear brighter in BSE mode. Higher magnification shows that the red pigment particles

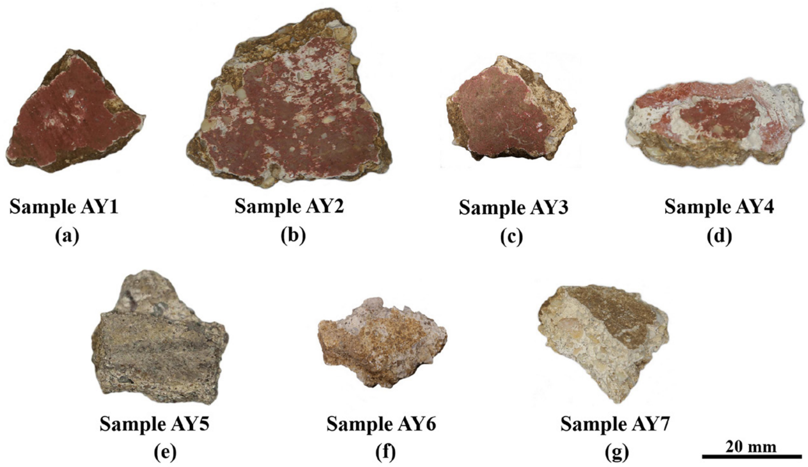

Figure 2. Hellenistic stucco fragments from Ashdod-Yam: (a) Sample AY1: dark red pigment; (b) Sample AY2: dark red pigment and areas of bright exposed plaster; (c) Sample AY3: dark red pigment with brown tone; (d) Sample AY4: two-layer fragment: upper layer of dark red pigment and areas of bright exposed plaster and bottom layer of dark red and bright red pigment and areas of exposed plaster; (e) Sample AY5: stripes of black pigment; (f) Sample AY6: plaster covered with soil remains; (g) Sample AY7: composite mortar base covered with plaster and brown soil remains.

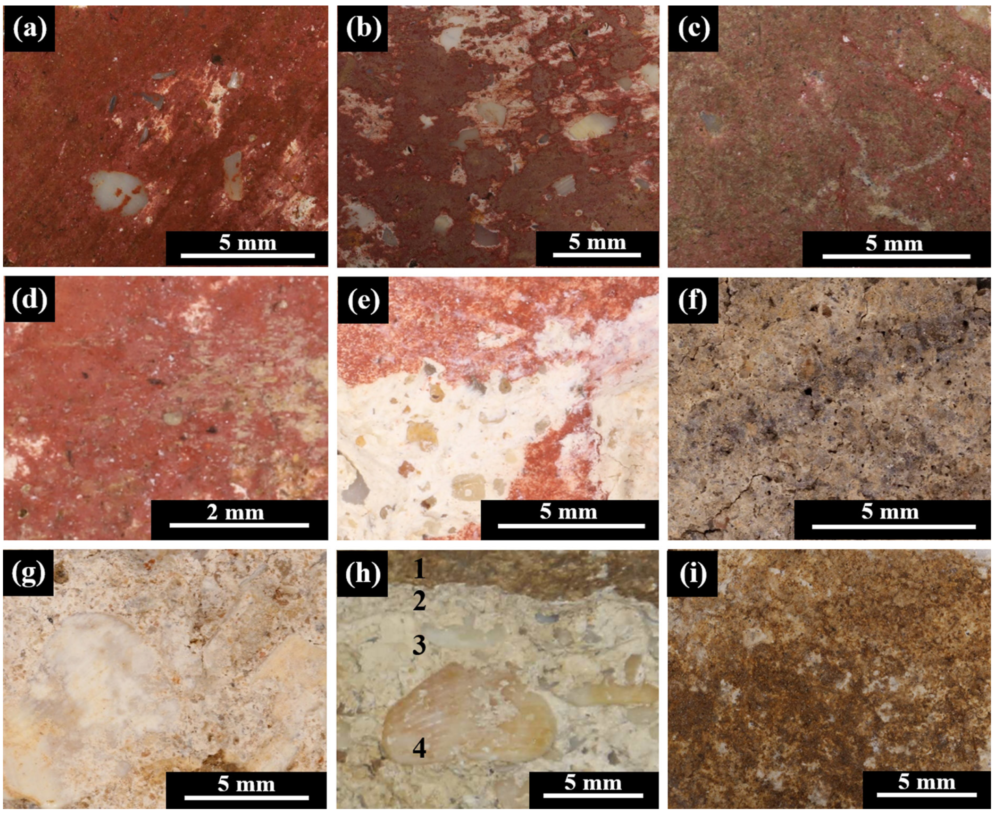

Figure 3. Catalogue of pigments, plaster, and mortar of Ashdod-Yam samples (Canon R6II camera): (a) Sample AY1: dark red paint and bright particles within plaster material (PS); (b) Sample AY2: dark red paint and areas of exposed bright plaster with different particles (PS); (c) Sample AY3: dark red paint with brown tone (PS); (d) Sample AY4: upper layer of dark red paint and areas of exposed bright plaster (PS); (e) Sample AY4: bottom layer of red paint and bright plaster with particles (PS); (f) Sample AY5: black stripe (PS); (g) Sample AY6: bright plaster with different particles (PS); (h) Sample AY 7: thin plaster layer (area 2) covered with brown soil (area 1), on top of composite mortar (area 3) with particles such as shells (area 4) (TCS); (i) Sample AY7: plaster covered with brown soil (PS).

Table 1. VT characteristics and macroscopic observation (Canon R6II camera) of Ashdod-Yam (AY), Yavneh-Yam (YY), and Tel Ya'oz (TY) stucco fragments.

Sample no.	Figure nos.	Description and preservation condition	Surface appearance and pigment color
AY1	Figs. 2a, 3a	Well-preserved pigment with minor erosion; fragments of seashells protruding beneath pigment layer	Dark red pigment, locally eroded, revealing underlying bright plaster
AY2	Figs. 2b, 3b	Moderate erosion; uneven pigment; fragments of seashells protruding beneath pigment layer	Dark red with brown tone; areas of exposed bright plaster
AY3	Figs. 2c, 3c	Slight cracking of surface layer; shell fragments exposed in eroded areas	Dark red with brown tone; surface cracks
AY4	Figs. 2d, 3d–3e	Preserved multi-layer structure; partial erosion; fragments of seashells protruding beneath pigment layer; various inclusions within plaster layer	Two-layer fragment: upper dark red, lower bright red with small white plaster areas
AY5	Figs. 2e, 3f	Moderate erosion; cracks on the surface; mineral inclusions dispersed throughout plaster	Black pigment in linear stripes (distinct decorative pattern) over plaster
AY6	Figs. 2f, 3g	Unpainted plaster surface; moderate erosion; mineral inclusions and seashell fragments dispersed throughout plaster	No pigment; plaster covered with soil residue
AY7	Figs. 2g, 3h–i	Moderate erosion; shell fragments and quartz particles; soil residue on top	White plaster layer over composite mortar base
YY1	Figs. 7a, 8a–b	Well preserved two-layer bright plaster; minor erosion along edges; quartz sand, shell fragments, and ceramic inclusions visible under higher magnification	Bright plaster layers separated by narrow red-painted strip; surface generally smooth with localized weathering
YY2	Figs. 7b, 8c–d	Two well-preserved plaster layers; slight surface flaking and fine cracks; mineral inclusions dispersed throughout plaster	Dark red pigment covering exterior; homogeneous color with some faded zones
YY3	Figs. 7c, 8e–f	Single moderately preserved plaster layer; minor detachment of paint from plaster; inclusions on fragment's back	Surface coated with dark red pigment; generally well-preserved but with minor discoloration and soil residue
TY1	Fig. 11a	Generally well-preserved; mineral inclusions dispersed throughout plaster	Plaster surface coated with dark red pigment
TY2.1	Fig. 11b	Generally well-preserved; mineral inclusions dispersed throughout plaster	Plaster surface coated with dark red pigment
TY2.2	Figs. 11b–c, 12a	Well-preserved plaster fragment; localized minor surface erosion	Coated with uniform red pigment layer; small exposed spots revealing underlying bright plaster
TY3	Figs. 11d, 12b	Generally well preserved; slight cracks and edge abrasion	Dark red pigment with matte surface; limited pigment loss along margins
TY4	Figs. 11e, 12c–d	Moderate preservation; back surface with sand particles, shell fragments, and ceramic inclusions	Red pigment coating mostly intact; localized fading and exposure of underlying plaster
TY5.2	Figs. 11f, 12e	Fragmented plaster in fair condition; visible inclusions on back	Red pigment layer with small, eroded areas; bright plaster visible in patches
TY5.3	Fig. 11h	Fair preservation	Red pigment with underlying bright plaster exposed in some areas
TY5.4	Figs. 11f, 12f	Compact; well-preserved; minimal flaking	Even red pigment with slight surface dullness; bright underlayer visible in minor cracks

Sample no.	Figure nos.	Description and preservation condition	Surface appearance and pigment color
TI6.1	Figs. 11k, 12g	Fair preservation; surface slightly abraded	Covered with red pigment showing mild fading; smooth overall texture
TI6.2	Figs. 11l, 12h	Good preservation; minor surface irregularities and some erosion	Red paint layer with subtle color variation
TI6.3	Fig. 11m	Fine mineral inclusions scattered throughout plaster	Uniform dark red pigment coat largely intact; bright plaster visible in eroded areas
TI6.4	Fig. 11n	Plaster material contains dispersed mineral inclusions	Uniform dark red pigment coat largely intact; bright plaster visible in eroded areas
TI6.5	Figs. 11o, 12i	Well-preserved; minor erosion exposing bright underlying plaster	Uniform dark red pigment coat largely intact; bright plaster noticeable in eroded areas
TI6.6	Fig. 11p	Mineral inclusions distributed throughout plaster	Dark red pigment with underlying plaster

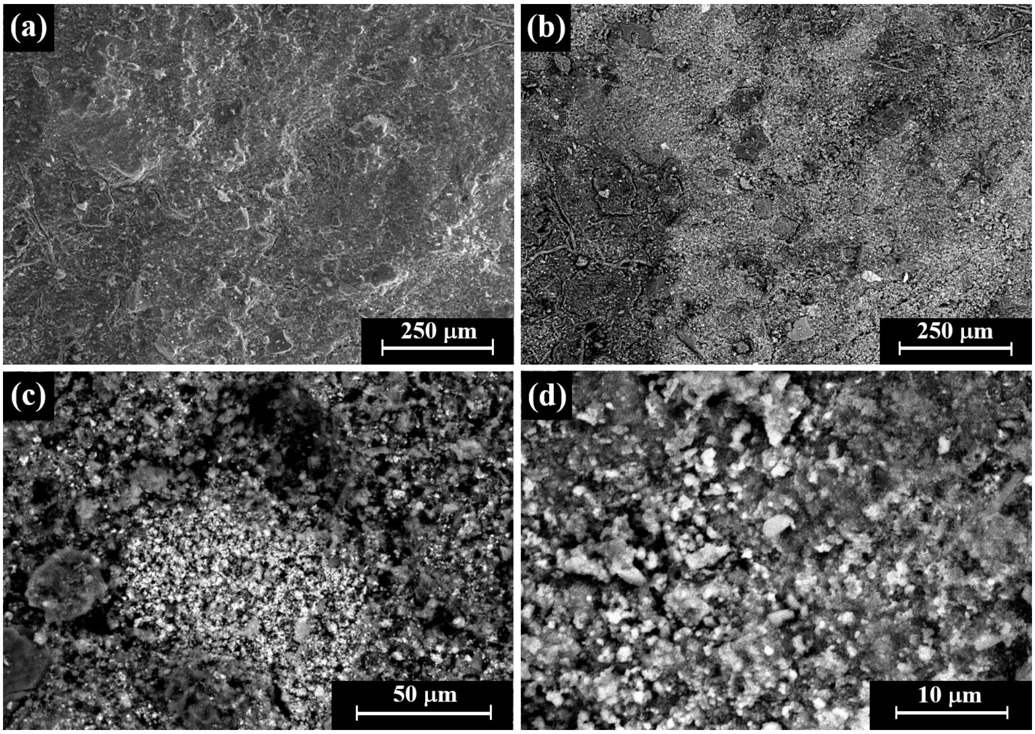

Figure 4. SEM images of the red paint on Sample AY4 (lower layer of the sample, PS) analyzed with EDS: (a, b) general view of the surface (SE and BSE modes, respectively); (c) higher magnification of the surface, where the bright area is dense with pigment particles (BSE mode); (d) higher magnification of bright red pigment particles (BSE mode).

range from 0.2 µm to 4 µm in diameter (Fig. 4d). The red pigments on samples AY1 and AY3 (Fig. 5a–b) display a similar brightness in BSE mode, consistent with Fe-rich oxide particles in the red pigment.

In contrast to the red pigment, the black-painted surface of Sample AY5 (Fig. 5c–d) appears darker in BSE mode, corresponding to a lower content of heavy elements. Higher magnification reveals the presence of organic fibers (Fig. 5d), suggesting that the black pigment is primarily organic in origin rather than mineral-based.

SEM-EDS analysis of the Ashdod-Yam samples (Appendix C, Table C1) reveals compositional differences between the red and black pigments and the surrounding plaster. The red pigment of Samples AY3 and AY4 consists mainly of Fe oxides, with variable contributions of Ca, Si, and aluminum (Al) oxides, and minor amounts of magnesium (Mg), potassium (K), titanium (Ti), and sulfur (S) oxides, consistent with a red ochre composition. The plaster matrices of Samples AY2, AY5, and AY6 are dominated by Ca and Si oxides, with smaller contributions of Al, Mg, Fe, and antimony (Sb) oxides.

VT of Sample AY5 indicates that the black pigment is worn, suggesting it was originally carbon-based. SEM-EDS analysis shows that the elemental composition of the black-painted areas is similar to that of the underlying plaster (mainly Ca, Si, Al, and Mg oxides), consistent with the known limitations of SEM-EDS in detecting carbon. No significant amounts of other mineral black pigments were detected, supporting the interpretation that the black pigment was most likely carbon based. The bright and dark contrasts observed in the BSE images are consistent with these compositional differences: lighter regions reflect heavier elements such as Fe, whereas darker regions represent the surrounding plaster.

FTIR analysis of Sample AY2 shows that the calcite is highly disordered, indicating a pyrogenic source. The thin black surface of Sample AY5 appears more ordered than the underlying layer, which is highly disordered. Sample AY6 presents borderline atomic order

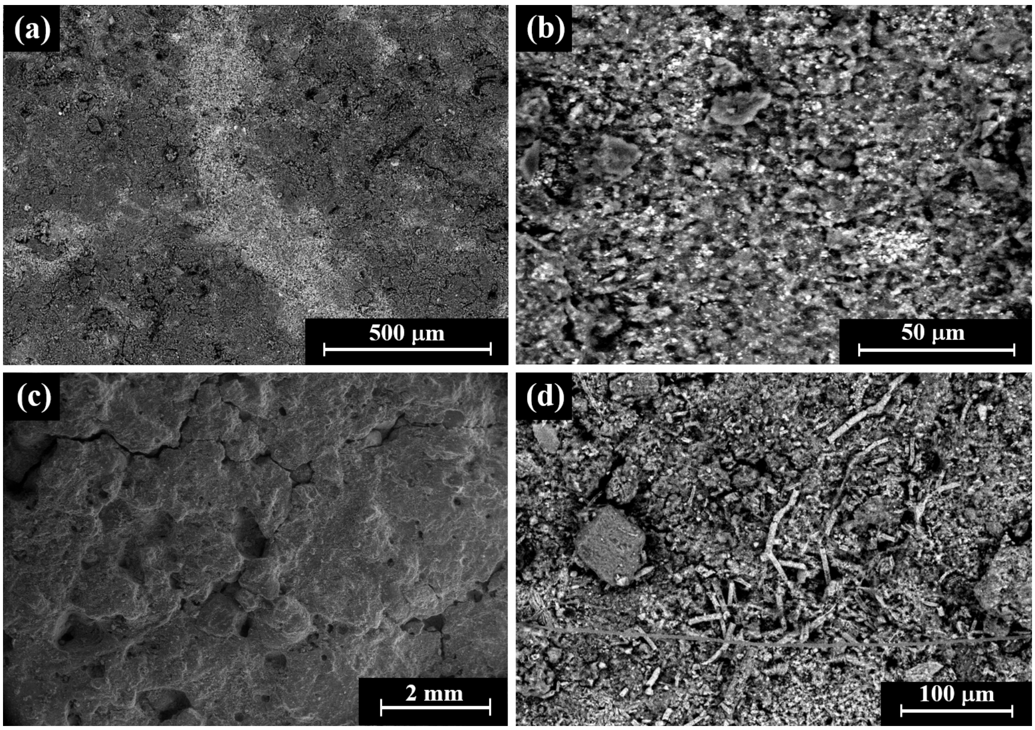

Figure 5. SEM images of the paint on AY samples (PS): (a) Sample AY3: surface, the bright areas are dense with red pigment particles (BSE mode); (b) Sample AY1: surface covered with red pigment particles (BSE mode); (c) Sample AY5: covered with black paint (SE mode); (d) higher magnifications of Fig. 5c, revealing the presence of organic fibers (BSE mode).

within the range between pyrogenic and geogenic calcite (Table 2). Sample AY7 was divided into several subsamples, all of which show highly disordered calcite, alongside clay and shell fragments (composed of aragonite) and quartz (Table 2). The degree of atomic order in calcite in all samples was assessed using FTIR grinding curves following Regev et al. (2010) (see Appendix D, Fig. D1).

Table 2. FTIR analysis of samples from Ashdod-Yam (AY), Yavneh-Yam (YY), and Tel Ya'oz (TY). Calcite atomic order was interpreted on the basis of grinding curves following Regev et al. (2010). Clay alteration due to exposure to elevated temperatures follows Berna et al. (2007). Ca = calcite; Cl = clay; (un) = unaltered; (a) = altered; Ar = aragonite; Q = quartz; G = gypsum.

Sample/Subsample no.	Description	Major minerals	Calcite order
AY2.1	Red pigment	Ca>>>>Cl	Disordered
AY2.2	White plaster	Ca	Disordered
AY2.3	Slightly translucent, plated gray-white inclusions in plaster	Ar	
AY5.1	Black surface	Ca	Ordered
AY5.2	Coarse black inclusions densely distributed (in plated layers) within the sandy plaster surface	Ca	Ordered
AY5.3	Sandy plaster layer underneath thin layer with coarse black inclusions	Ca>>Q	Disordered
AY6.1	White plaster bulk	Ca>Ar>>>Q,Cl	Ordered
AY6.2	Yellow-brown patches	Cl(un),Ca>Q	
AY7.1	Smooth white plaster bulk surface	Ca>>>Q,Cl(al)	Disordered
AY7.2	Flat shell inclusion aligned with plaster surface	Ar	
AY7.3	Sandy red-brown sediment adhering to plaster fragment	Cl(un)>Q>>Ca	
AY7.4	Coarse white plaster with many inclusions	Ca>>>>Q	Disordered
YY1.1	Small red pigment patch	Ca	Highly disordered
YY1.2	Crumbly white plaster bulk with coarse sand and some irregular yellowish discoloration	Ca>>>>Q	Highly disordered
YY2.1	Red pigment surface	Ca>>>Q>Cl	Highly disordered
YY2.2	White sandy plaster with some yellow-brownish discoloration (upper layer of sample YY2)	Ca>Q	Highly disordered
YY2.3	Thinner brighter white layer (lower layer of sample YY2)	Ca>>>Q	Highly disordered
YY3.1	Red pigment surface	Ca	Borderline
YY3.2	Bright white powdery plaster with coarse inclusions	Ca	Borderline
TY1.1	Red pigment surface	Ca>>>>Q	Ordered/borderline
TY1.2	Hard white plaster with opaque white inclusions	Ca	Borderline
TY1.3	Bright thin white plaster layer	Ca	Borderline
TY2.1	Red pigment, angled surface	Ca>>>>Cl(un)	Disordered
TY2.2	Powdery white with coarse inclusions underneath pigment	Ca	Disordered
TY2.3	Orange-brownish sediment adhering to plaster	Ca>>>Q>Cl	Ordered
TY3.1	Relatively thick red pigment surface	Ca>>>>Q	Ordered/borderline
TY3.2	Hard white plaster with many coarse sand-sized inclusions	Ca	Borderline
TY4.1	Red pigment surface	Ca>>>>Q	Ordered
TY4.2	Brittle powdery white plaster with coarse inclusions	Ca	Ordered

XRD analysis of the red paint on Sample AY1 (Fig. 6a) reveals crystalline phases of calcite, hematite, quartz, and Cu. The presence of hematite, calcite, and quartz is typical of red ochre pigment, composed of hematite mixed with calcite and quartz sand particles; hematite may have been mixed with lime to achieve pink tints (Ashkenazi et al., 2021; Asscher et al., 2025). The presence of Cu in the XRD results may reflect activities involving copper carried out at Ashdod-Yam.

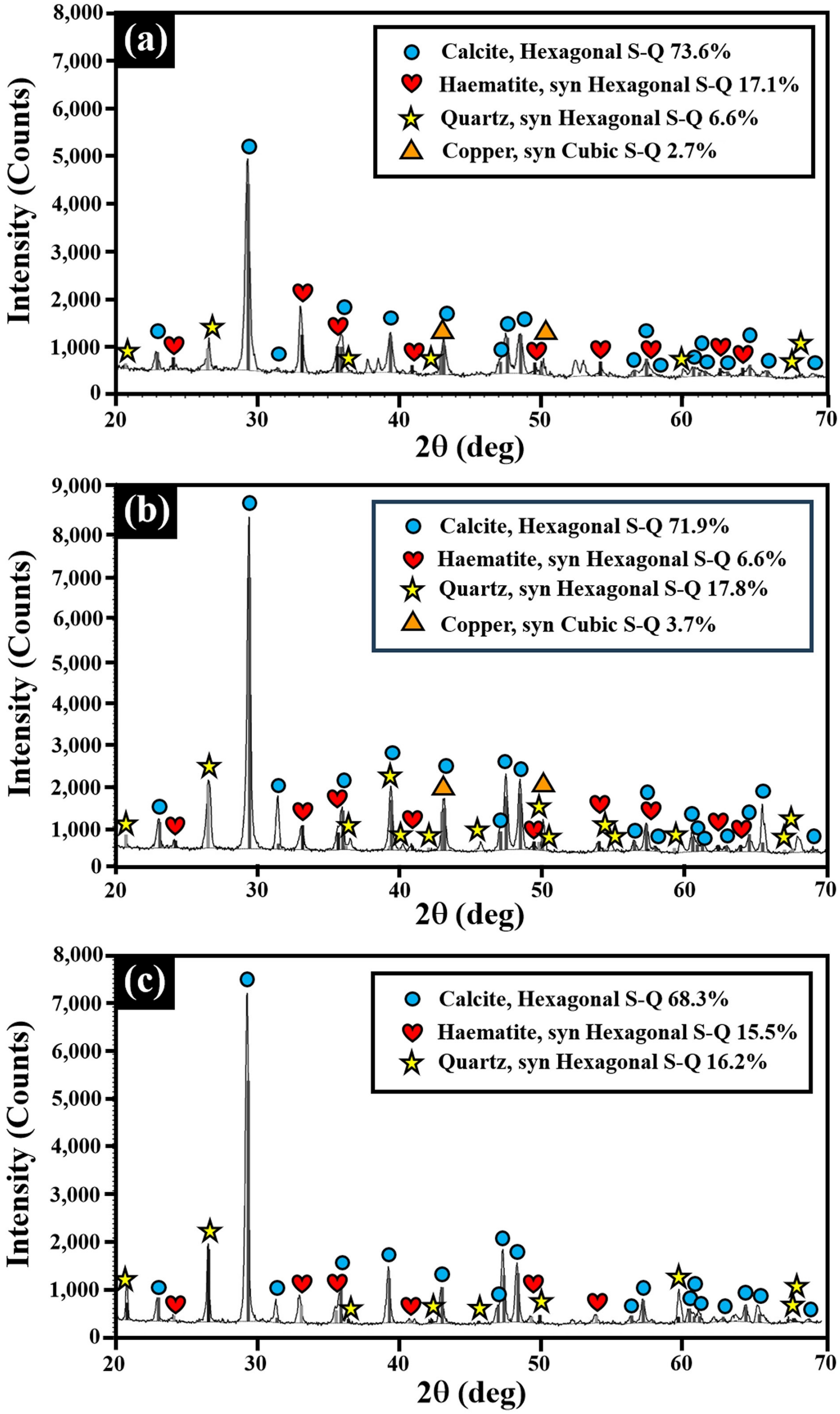

Figure 6. XRD analysis results of red paint on (a) Sample AY1, (b) Sample YY3, and (c) Sample TY6.

3.2 The *stucco* fragments from Yavneh-Yam (YY)

VT (Fig. 7) and macroscopic observations (Fig. 8) were conducted to examine the stucco fragments from Yavneh-Yam. A general description of the samples is provided here. The fragments share several characteristics, including red-painted layers applied over bright plaster substrates and the presence of mineral, shell, and ceramic inclusions. Differences observed in pigment intensity, layering arrangement, and surface condition likely reflect variations in decorative considerations and/or post-depositional alteration rather than differences in production techniques. In summary (Figs. 7a–c, 8a–f), Sample YY1 exhibits two plaster layers separated by a red-painted stripe; Sample YY2 consists of two plaster layers covered with dark red

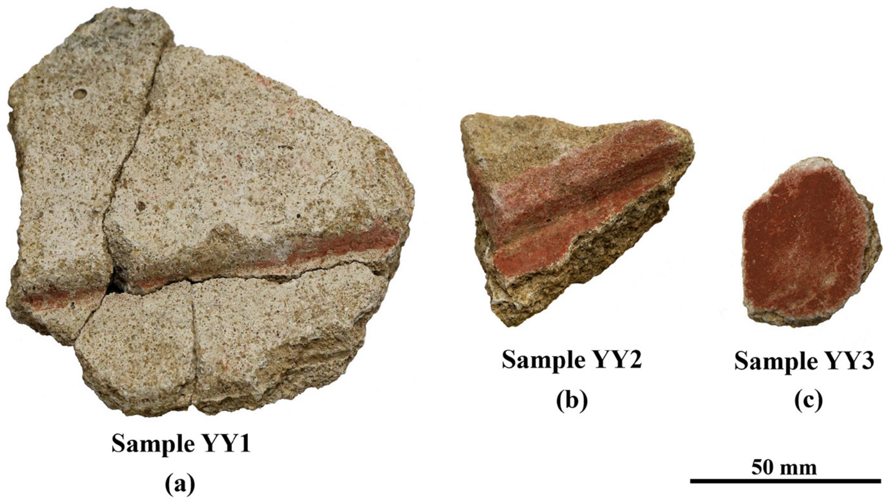

Figure 7. Hellenistic stucco fragments from Yavneh-Yam (YY): (a) Sample YY1: two layers of bright plaster and a painted red stripe between them; (b) Sample YY2: two layers of plaster covered with dak red color; (c) Sample YY3: plaster covered with dark red color.

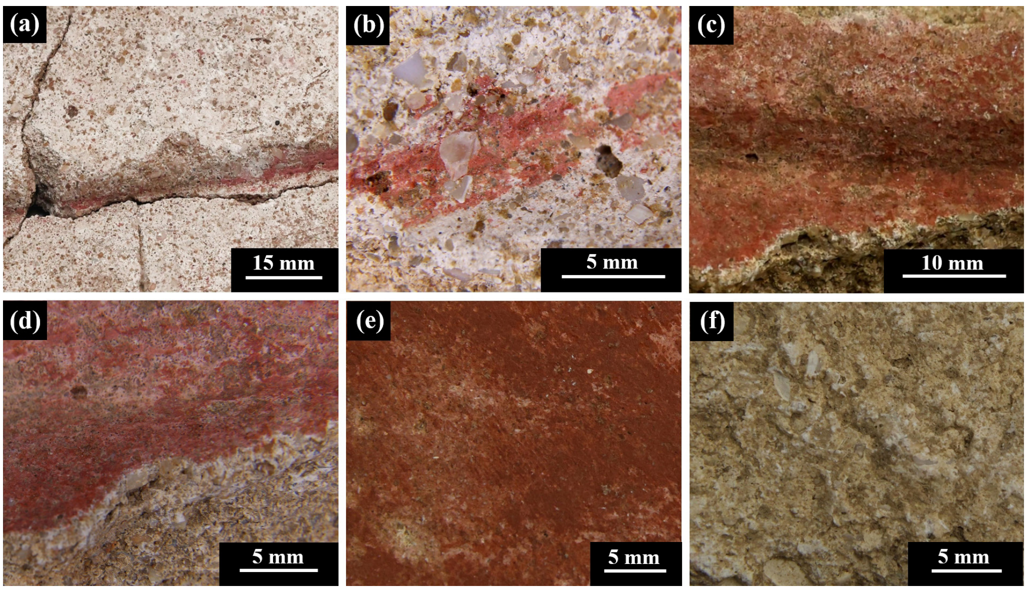

Figure 8. Catalogue of pigments and plaster of Yavneh-Yam Samples (Canon R6II camera): (a) Sample YY1: two layers of bright plaster (PS) and a painted red stripe between them (TCS); (b) higher magnification of the plaster layers and painted red stripe with different particles; (c) Sample YY2: two layers of plaster covered with dark red paint (PS); (d) higher magnification of dark red paint (PS); (e) Sample YY3: dark red paint cover (PS); (f) Sample YY3: plaster on back of the sample (PS).

pigment; and Sample YY3 is a plaster fragment coated with dark red pigment. High-magnification observations reveal particles such as quartz sand, shell, and ceramic inclusions in several samples. A concise overview of the VT and macroscopic observations is presented in Table 1 (YY samples).

SEM observations of the red-painted surfaces of the Yavneh-Yam samples reveal compositional and textural contrasts between the pigment and the plaster. On the red-painted surface of Sample YY1 (Fig. 9a), the pigment zones appear brighter than the surrounding plaster in BSE mode, reflecting a higher concentration of heavy elements—primarily Fe in the form of Fe oxides—relative to the Ca- and Si-oxide-based plaster. At higher magnification, needle-like dark particles up to 50 µm in length and bright Fe-oxide pigment crystals ranging between 0.4 µm and 5 µm in diameter were observed (Fig. 9a–b, BSE mode). The red-painted surface of Sample YY2 exhibits a rough texture in SE mode (Fig. 9c) and a bright surface with darker particles in BSE mode (Fig. 9d–e). The bright regions correspond to Fe-oxide pigment crystals, whereas

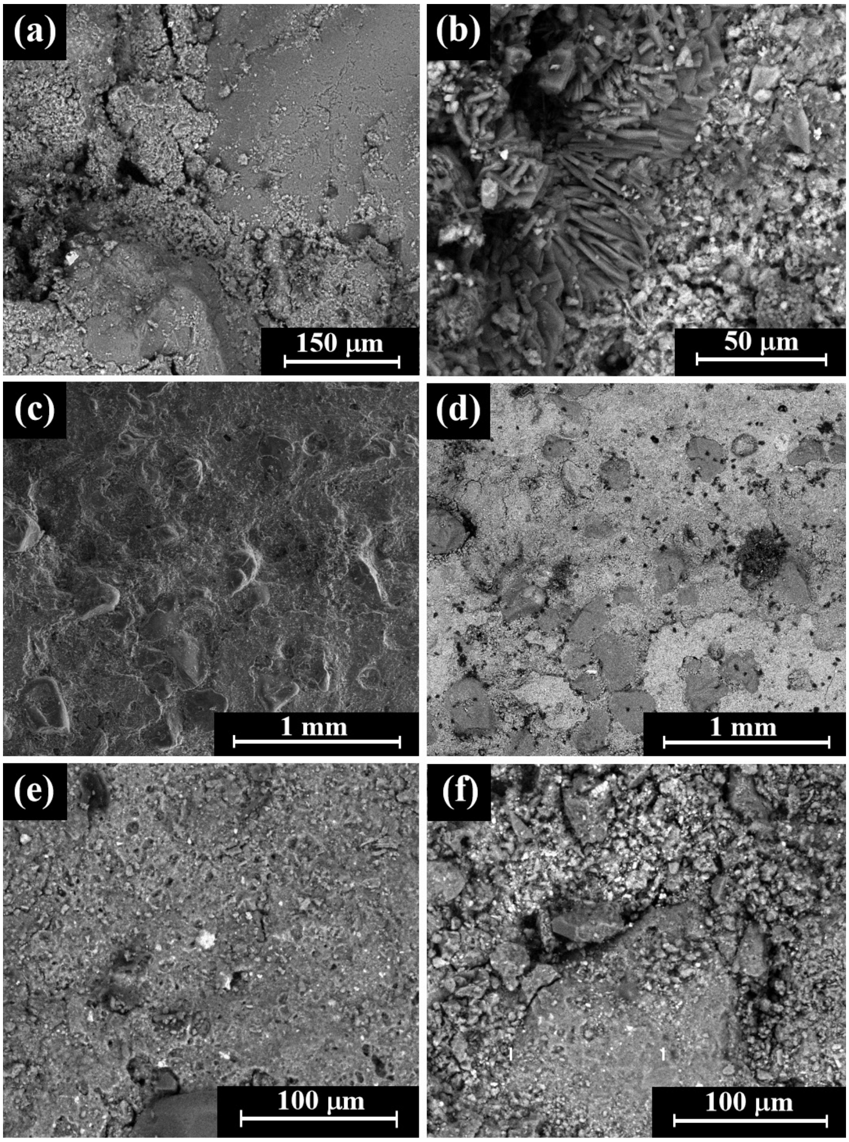

Figure 9. SEM images of paint from Yavneh-Yam stucco fragments (PS): (a–b) surface of Sample YY1 covered with red paint (right side of the sample in BSE mode); (c–d) upper layer of Sample YY2 covered with dark red paint (SE mode and BSE mode, respectively); (e) higher magnification of Fig. 7d (Sample YY2, BSE mode) showing bright red pigment particles; (f) surface of Sample YY3 covered with dark red pigment (bright particles in BSE mode).

the darker particles are consistent with the lighter Ca- and Si-oxide-based plaster. Similarly, Sample YY3 (Fig. 9f) shows bright red pigment particles, ranging from less than 1 µm to 8 µm, together with large, darker inclusions up to 150 µm in diameter, likely representing plaster aggregates or impurities.

SEM-EDS elemental spectra of the plaster and pigment layers from samples YY1–YY3 reveal clear compositional differences between the two materials. The plaster layer of Sample YY2 (Fig. 10a, upper layer) consists mainly of Ca, Si, and oxygen (O), with secondary elements including Al and Mg. This composition suggests a lime-based plaster mixed with quartz components, likely originating in added sand particles—a common practice to increase mechanical strength and durability of lime plasters (Ali and Elrahim, 2021; Arizzi and Cultrone, 2021). In contrast, the dark red paint of Sample YY2 (Fig. 10b, upper layer) displays additional peaks of Fe, S, and K, consistent with the use of an Fe-based pigment phase. Similarly, the spectrum of the dark red pigment particles from Sample YY3 (Fig. 10c) displays additional peaks of Fe, Al, and sodium (Na).

EDS analysis results for Samples YY1–YY3 (Appendix C, Table C2) supports these observations, showing that the plaster is dominated by Ca and Si oxides, whereas the red pigment layers are enriched in Fe oxides alongside Ca, Si, and Al oxides, with minor amounts of Mg, K, S, and phosphorus (P) oxides. These results emphasize the compositional distinction between the lime-based plaster and the Fe-rich red pigment, consistent with the use of red ochre.

XRD analysis of the red paint pigment on the YY samples (Fig. 6b, Sample YY3) produced results similar to those from Ashdod-Yam, revealing crystalline phases of calcite, hematite, quartz, and Cu.

FTIR analysis shows that both plaster and pigments in Samples YY1 and YY2 contain highly disordered calcite, indicative of pyrogenic formation. The plaster and pigment in Sample YY3 exhibit borderline atomic order between the geogenic and pyrogenic ranges (Table 2). The degree of calcite atomic order for the Yavneh-Yam samples was assessed using FTIR grinding curves following Regev et al. (2010) (see Appendix D, Fig. D2).

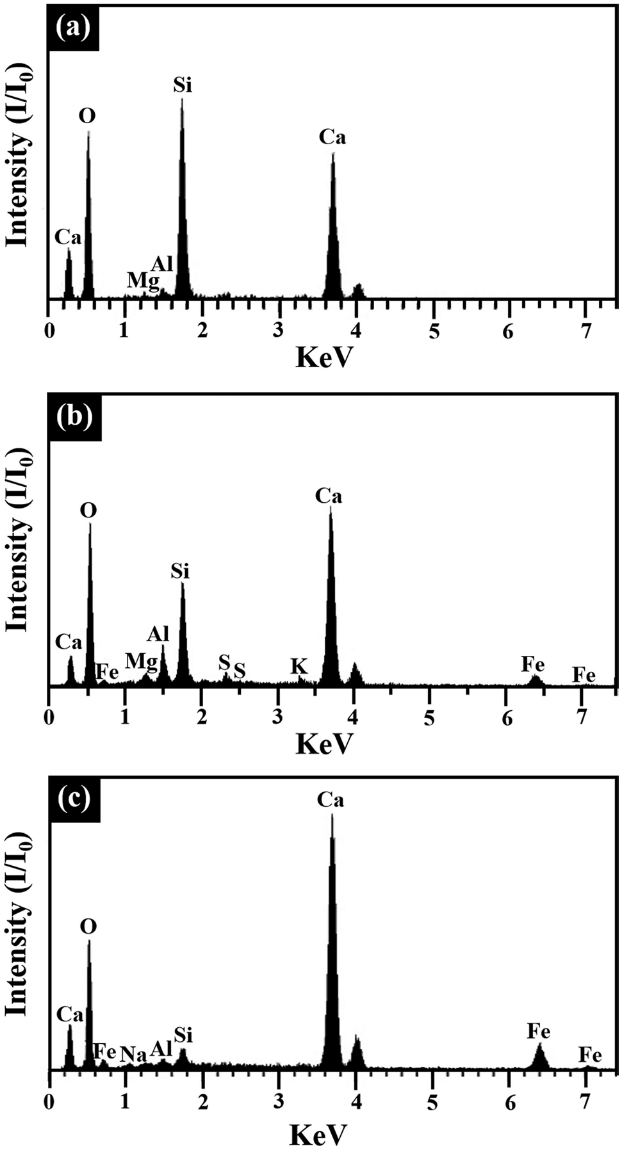

Figure 10. SEM-EDS elemental spectra of the Yavneh-Yam samples: (a) Sample YY2: peaks of the plaster (upper layer); (b) Sample YY2: peaks of the dark red paint (upper layer); (c) Sample YY3: peaks of the dark red paint.

3.3 The stucco fragments from Tel Ya‘oz (TY)

VT (Fig. 11) and macroscopic observation (Fig. 12) were conducted to examine the stucco fragments from Tel Ya‘oz. A macroscopic description of the samples is provided below. The fragments are generally well preserved and exhibit a consistent use of red pigment applied over bright plaster layers. Minor variations in pigment tone and surface preservation were observed among the

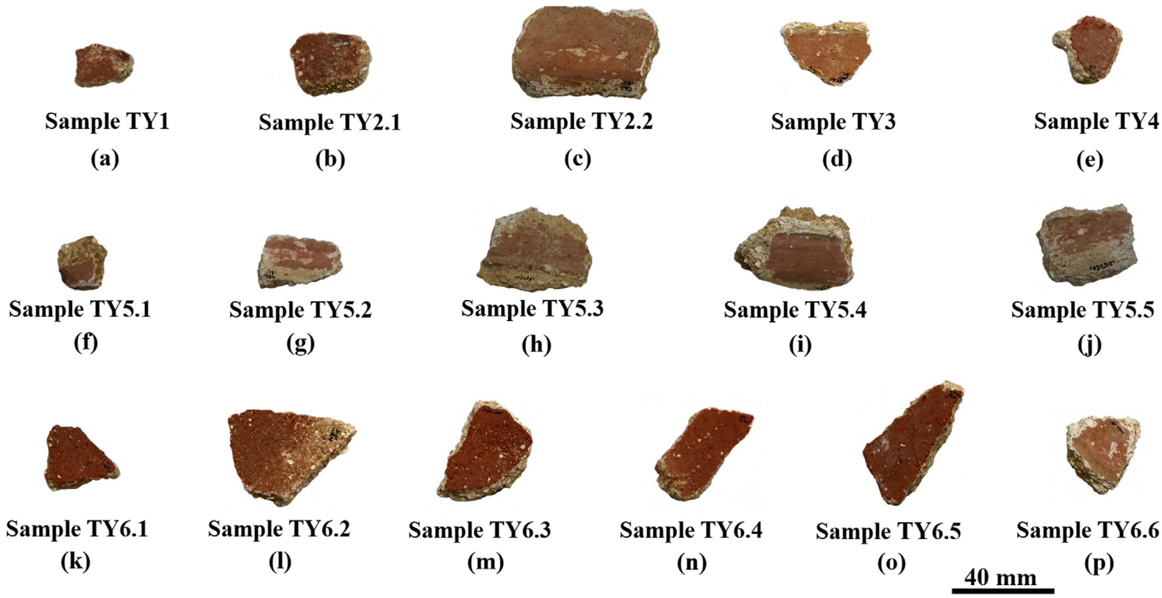

Figure 11. Hellenistic stucco fragments from Tel Ya'oz with dark red paint: (a) Sample TY1; (b–c) fragments of Sample TY2; (d) Sample TY3; (e) Sample TY4; (f–j) fragments of Sample TY5; (k–p) fragments of Sample TY6.

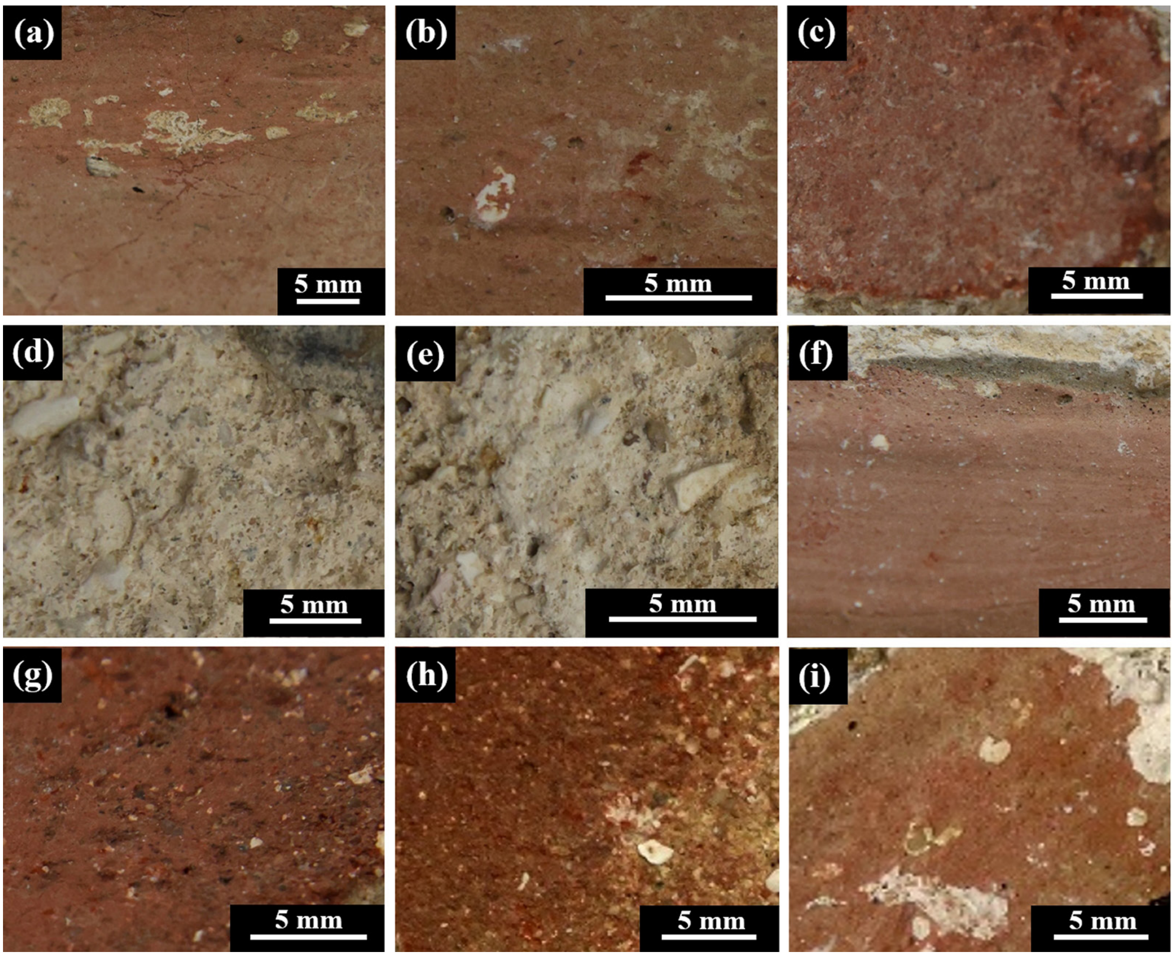

Figure 12. Catalogue of pigments and plaster of Tel-Ya'oz samples (Canon R6II camera): (a) Sample TY2.2: red paint; (b) Sample TY3: red paint; (c) Sample TY4: red paint; (d) Sample TY4: plaster on the back of sample; (e) Sample TY 5.2: plaster on the back of sample (f) Sample TY5.4: red paint; (g–h) Samples TY6.1 and TY6.2: red paint; (i) Sample TY6.5: red paint overlying bright plaster.

samples (Figs. 11a–p, 12a–i). Several samples (Samples TY4 and TY5.2) contain inclusions such as quartz sand, shell fragments, and ceramic inclusions within the plaster matrix, particularly visible on the back surfaces (Fig. 12d–e). A summary of the macroscopic and visual characteristics is presented in Table 1 (TY samples).

SEM observations of the red-painted surface of Sample TY1 reveal bright islands of red pigment surrounded by darker plaster material in BSE mode (Fig. 13a), indicating a higher content of heavy elements (mainly Fe oxides) within the pigment, relative to the surrounding Ca- and Si-oxide-based plaster. The surface appears rough in SE mode (Fig. 13b). Dark particles within the plaster reach diameters of up to 500 µm (Fig. 13a, c–d, BSE mode). The SEM-EDS elemental spectrum of the dark red pigment of Sample TY1 (Fig. 14a) reveals the presence of Fe, Ca, O, Si, Al, and arsenic (As). The dark red pigment of Sample TY3 (Fig. 14b) similarly contains Fe, Ca, O, Si, Al, and Ti. These results indicate that the pigments are enriched in Fe oxides, consistent with red ochre.

SEM observation of the plaster of Sample TY2 reveals a rough surface with particles up to 300 µm in diameter (Fig. 15a, SE mode). Both dark and bright particles are present. The bright areas correspond to regions enriched with elements of higher atomic weight (mainly Fe oxides), whereas the dark areas represent regions richer in lighter elements, primarily Ca and Si oxides forming the plaster. The bright particles range between 0.5 µm and 20 µm, while the darker ones vary from a few micrometers up to 30 µm (Fig. 15b, BSE mode). The red-painted exterior of Sample TY6 also displays a rough surface (Fig. 15c, SE mode). In BSE mode, bright areas of red pigment stand out clearly against the darker plaster background, reflecting the contrast between Fe-bearing pigment and the lighter Ca and Si oxides in the plaster. The bright pigment particles range from 0.3 µm to 8 µm in diameter (Fig. 15d). Sample TY3 similarly shows the red-painted surface brighter than the surrounding plaster in BSE mode (Fig. 16a–b), again reflecting compositional contrast between Fe-bearing pigment particles and the lighter Ca- and Si-oxide-based plaster. At higher

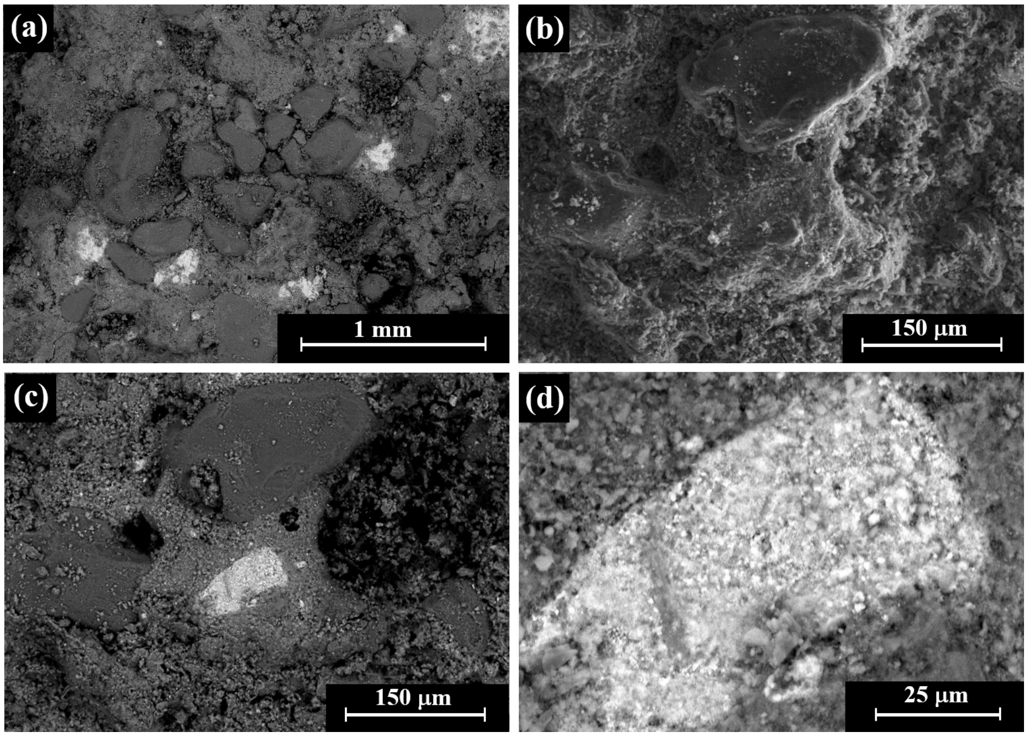

Figure 13. SEM images of red paint of Sample TY1 (PS): (a) plaster (dark in BSE mode) and dark red pigment (bright spots in BSE mode); (b–c) higher magnifications of plaster overlaid by areas of dark red pigment (in SE and BSE modes, respectively); (d) higher magnification of dark red pigment (bright area in BSE mode).

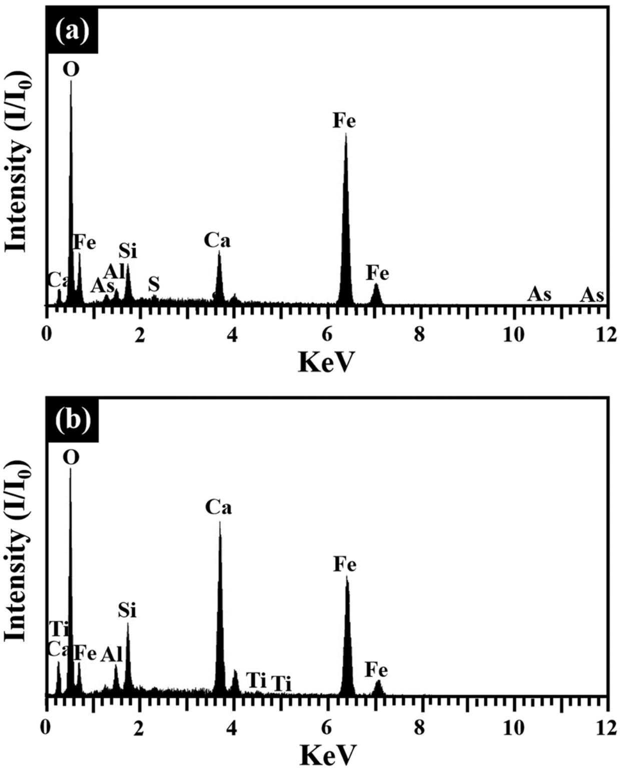

Figure 14. SEM-EDS elemental spectra of Tel-Ya'oz samples showing peaks of dark red paint: (a) Sample TY1; (b) Sample TY3.

magnification, SE mode imaging reveals a rough surface texture (Fig. 16c), while BSE mode shows bright Fe-oxide pigment particles ranging from 0.3 μm to 9 μm in diameter (Fig. 16d).

SEM-EDS analysis of the plaster and red pigment of the Tel Ya'oz samples reveals clear compositional distinctions between the two materials. The plaster of samples TY1 and TY2.1 (Appendix C, Fig. C3) is dominated by Ca and Si oxides, with minor amounts of Fe, Al, Mg, and K oxides. In contrast, the red pigment layers of samples TY1, TY2, TY3, and TY6.1 (Appendix C, Table C3) are enriched in Fe oxides, along with Ca, Si, and Al oxides, and contain minor amounts of Mg, K, S, Ti, and As oxides. These results support the identification of the red pigment as Fe-based red ochre.

XRD analysis of the red paint pigment on the Tel Ya'oz samples (Fig. 6c, Sample TY6) reveals crystalline phases of calcite, hematite, and quartz, typical of red ochre pigments composed of hematite mixed with calcite and quartz sand.

FTIR analysis reveals that the plaster and pigments of Sample TY1 show borderline atomic

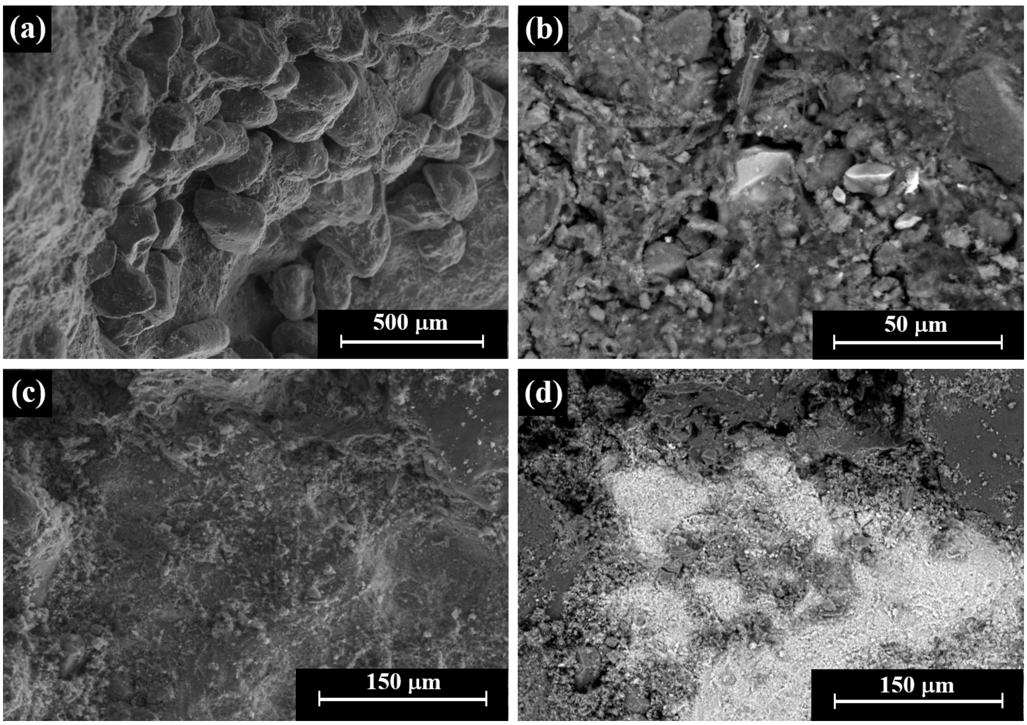

Figure 15. SEM images of red paint from the Tel-Ya'oz samples (PS): (a) Sample TY2: plaster (SE mode); (b) Sample TY2: plaster with red pigment particles (BSE mode); (c) Sample TY6: surface (SE mode); (d) Sample TY6: dark area of plaster and bright area of red pigment (BSE mode).

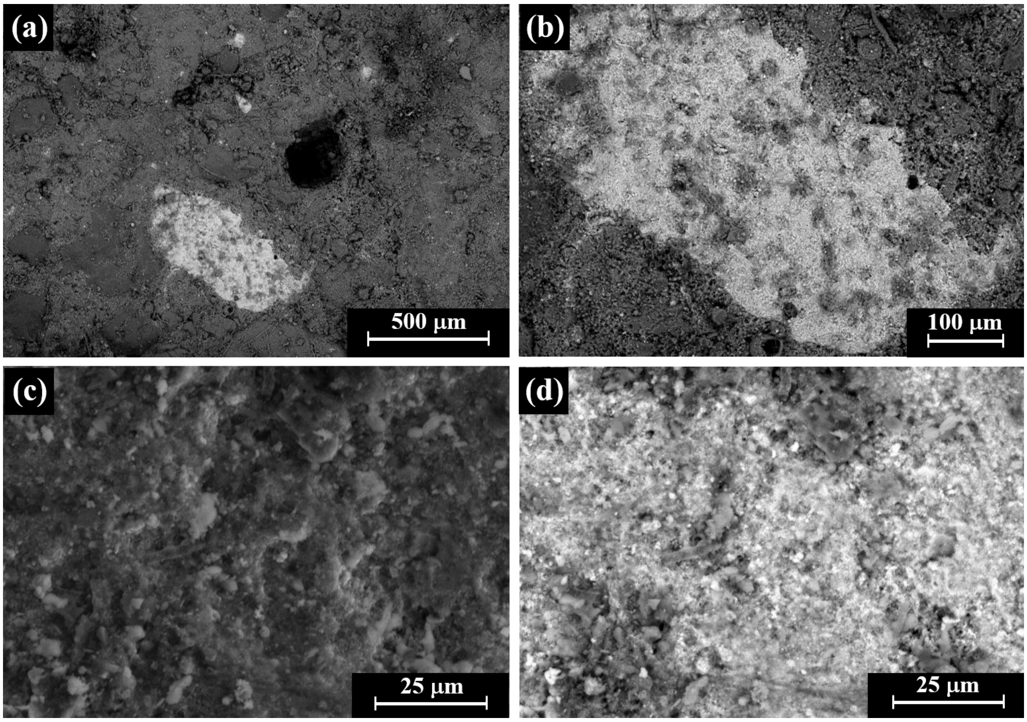

Figure 16. SEM images of Sample TY3 (PS): (a) plaster with red pigment spots (BSE mode); (b) higher magnification of red pigment area (BSE mode); (c–d) higher magnification of red pigment particles (SE mode and BSE mode, respectively).

order between the geogenic and pyrogenic ranges. The plaster and pigment of Sample TY2 exhibit calcite with a high degree of atomic disorder, associated with pyrogenic formation, while the sediment attached to the plaster shows calcite atomically ordered within the geogenic range. The plaster and pigment of Sample TY3 show borderline atomic order within the geogenic and pyrogenic ranges, while the plaster and pigment of Sample TY4 display calcite atomically ordered within the geogenic range (Table 2). The degree of atomic order of calcite in the Tel Ya'oz samples was assessed using FTIR grinding curves following Regev et al. (2010) (see Appendix D, Fig. D3).

4. Discussion

Stucco wall fragments from Ashdod-Yam, Yavneh-Yam, and Tel Ya'oz were analyzed to obtain information on their microstructure, composition, phases, manufacturing methods, and raw material sources. The objective of this study is to determine whether the southern coast of Palestine reflects a distinct know-how of Hellenistic stucco decoration. Such an investigation contributes to understanding the technological and ornamental *koiné* of the Hellenistic southern Levant.

VT and SEM-EDS analysis indicate that the plasters from Hellenistic strata at all three sites consist predominantly of calcite, with notable amounts of silica, reflecting the use of a lime-based binder combined with various aggregate minerals. These aggregates, including quartz sand, shell fragments, and ceramic inclusions, likely contributed to the mechanical stability and textural characteristics of the plaster and mortar (Figs. 3g–h, 8a–b, f, 12d–e, Appendix C, Tables C1–C3).

VT and macroscopic inspection (color catalogues, Figs. 3, 8, 12) suggest that the red pigment is based on red ochre, while the black pigment, which is relatively worn, is likely carbon black-based. SEM observations in BSE mode show red-painted areas brighter than the surrounding plaster, reflecting the higher atomic number of Fe in the pigment relative to Ca in the plaster. Black-painted areas exhibit minimal contrast with the plaster, consistent with the low atomic number of carbon, which is also difficult to detect quantitatively by SEM-EDS.

SEM-EDS analysis of plaster and mortars reveals a composition dominated by CaO, with contributions of

SiO_2, Fe_2O_3, Al_2O_3, and MgO, corresponding to quartz, clay, and ceramic inclusions. SEM-EDS results confirm that red pigments are composed mainly of Fe oxide, typical of red ochre (Mateos et al., 2018; Miriello et al., 2018; Marketou et al., 2019; Ashkenazi et al., 2021; Tarassova and Tarassov, 2023; Teklay et al., 2023; Cortea et al., 2024). The black pigment shows a composition very similar to that of the plaster, including CaO, SiO_2, Fe_2O_3, Al_2O_3, MgO, and P_2O_5 (Appendix C, Tables C1–C3). This compositional similarity, combined with the worn appearance of the black paint, supports its identification as carbon black rather than a mineral-based pigment such as a manganese (Mn) oxide. The absence of detectable Mn in the SEM-EDS spectra reinforces this interpretation.

FTIR analysis suggests that several plaster samples were not made from fully reacted lime. While some samples have highly disordered calcite, which can be associated with pyrogenic lime, others show borderline or ordered atomic arrangements within the geogenic range. Several explanations are possible: builders may have preferred crushed limestone or chalk to lime; production temperatures may have been too low to complete the lime cycle; or post-depositional processes may have increased the degree of atomic order of originally pyrogenic lime over time. Current evidence is insufficient to determine the most likely scenario (Poduska et al., 2012).

FTIR results suggest that the plasters from Yavneh-Yam were produced using primarily pyrogenic lime, as indicated by the highly disordered calcite, whereas plasters from Ashdod-Yam and Tel Ya'oz contain mixtures of lime and non-lime materials, including geogenic calcite. This distinction may reflect differences in local raw material availability, production techniques, or intended plaster quality and durability. Incomplete lime reactions or deliberate inclusion of geogenic carbonate may point to technological limitations, alternative building practices, or differences among workshop traditions.

XRD results show that the red pigment from all three sites was most likely produced near Ashdod, aligning with the local availability of *ḥamra*, a natural Fe-rich soil suitable for red ochre production (Sandler et al., 2023). This suggests a regional network of pigment procurement and possibly centralized workshops supplying multiple sites along the southern Levantine coast. The combination of locally produced lime-based plasters and mortars with regionally sourced pigments highlights the interplay between local production techniques and broader material exchange networks during the Hellenistic period.

The analyzed fragments can be assigned to the "Masonry Style" or "First Pompeian Style", typical of the Hellenistic period in the Levant (Laidlaw, 1985; Ling, 1991: 12–99; Rozenberg, 2008: 283–298). This style, imitating stone masonry in plastered relief, has been identified at Levantine Hellenistic sites, including Jebel Khalid, Syria (Jackson, 2016), and Beth Yeraḥ/Philoteria (Tal and Reshef, 2017: 28–30) and Tel Anafa (Kidd, 2018) in Israel. Similar techniques are attested also at later Herodian/Early Roman and Roman sites in Judaea (Foerster, 1995; Rozenberg, 2008). In comparison, red, yellow, and brown pigments from Tell Iẓṭabba were produced locally in the Beth She'an Valley (Maeir, 2020; Ashkenazi et al., 2021), and their wider variety and higher quality (Appendix E, Table E1) suggest more advanced technological capabilities than those at the sites in the Ashdod region (Table 2).

Technical preferences in plaster, mortar, and pigment production reflect not only functional considerations but also social and cultural meanings. Within production contexts, such choices can be understood through the framework of "communities of practice" (Lave and Wenger, 1991; Wendrich, 2012; Steidl, 2020; Lorenzon, 2023), in which knowledge is transmitted conservatively across time and space (Roux, 2015). Technological path dependency (David, 1985) may explain the persistence of certain production practices.

The consistency of the red pigment source across sites, combined with local plaster and mortar production, suggests a degree of standardization in material selection and preparation. This may indicate centralized workshops or shared production knowledge in the Ashdod region. Whether additional Hellenistic southern coastal sites such as Ashkelon (Birney, 2017) and Gaza (Humbert, 2012) reflect the same workshop expertise remains to be determined.

Overall, the stucco fragments from Ashdod-Yam, Yavneh-Yam, and Tel Ya'oz demonstrate a regional Hellenistic tradition characterized by local plaster and mortar production combined with standardized pigment use, consistent with the "Masonry Style" and representative of both technological and social aspects of wall decoration.

Taken together, the applied methodology enables a comprehensive characterization of the plasters and pigments from the southern Coastal Plain Hellenistic sites of Ashdod-Yam, Yavneh-Yam, and Tel Ya'oz. The results confirm the use of red ochre and carbon black-based pigments, reveal compositional differences between plasters and pigments, and indicate predominantly local production practices. Overall, the study successfully addresses the central research question, achieving its objectives and providing new insights into the technological expertise and decorative practices of Hellenistic stucco production along the southern Levantine coast.

5. Conclusions

Although all analyzed stucco fragments can be categorized as belonging to the “Masonry Style” from a decorative standpoint, indicating a certain level of standardization in their technological production, our findings reveal a more complex situation.

The plaster and mortar of all stucco fragments from Ashdod-Yam, Yavneh-Yam, and Tel Ya'oz were composed of calcite mixed with various aggregates. The examined plaster and samples from Yavneh-Yam (with the exception of Sample YY3) exhibit a disordered calcite structure, indicative of good quality plasters. In contrast, the plaster and mortar samples from Ashdod-Yam and Tel Ya'oz show greater variability in calcite atomic order, indicating a lower level of standardization. The red paints of all stucco fragments from the three sites were produced with red ochre, whereas the black paint was most probably created using a carbon black-based pigment. At all three sites, pigments were mixed with fine plaster powder.

Based on the combined visual, chemical, and mineralogical results, materials used in plaster, mortar, and pigment production appear consistent with locally available sources, although alternative provenances cannot be entirely ruled out. The technological communities of practice involved in the production of painted stucco in the southern Coastal Plain of Palestine during the 2nd century BCE were likely influenced and informed by a shared Graeco-Phoenician tradition. Nonetheless, the variability observed in certain production aspects indicates a level of flexibility and adaptation that varied from site to site.

Further analyses of the Hellenistic painted stucco from additional micro-regions within Palestine and the broader Levant are essential for developing a more nuanced understanding of this technological and artistic tradition.

References

Ali, M.F., Elrahim, A.M., 2021. Analytical study of the blue pigment used in Ottoman house mural paintings, Cairo, Egypt. *Scientific Culture* 7 (3), 41–51. https://doi.org/10.5281/zenodo.4916497.

Ali, M.F., Youssef, M.M., 2020. An analytical study of a mural with colorful geometric decoration, Coptic Museum, Cairo, Egypt: a case study. *Scientific Culture* 6 (3), 37–52. https://doi.org/10.5281/zenodo.3956807.

Amadori, M.L., Barcelli, S., Poldi, G., Ferrucci, F., Andreotti, A., Baraldi, P., Colombini, M.P., 2015. Invasive and non-invasive analyses for knowledge and conservation of Roman wall paintings of the villa of the Papyri in Herculaneum. *Microchemical Journal* 118, 183–192. https://doi.org/10.1016/j.microc.2014.08.016.

Amadori, M.L., Vagnini, M., Vivani, R., Anselmi, C., Chaverdi, A.A., Callieri, P., Matin, E., Mengacci, V., 2021. Advances in characterization of colourful residues unearthed in Persepolis West craft zone using microscopic and spectroscopic techniques. *Microchemical Journal* 167, 106304. https://doi.org/10.1016/j.microc.2021.106304.

Apostolaki, C., Perdikatsis, V., Repuskou, E., Brecoulaki, H., Lepinski, S., 2006. Analysis of Roman wall paintings from ancient Corinth/Greece, in: Agioutantis, Z.G., Komnitsas, K. (Eds.), *Book of Proceedings: 2nd International Conference on Advances in Mineral Resources Management and Environmental Geotechnology*. Heliotopos Conferences, Athens, pp. 729–734.

Arizzi, A., Cultrone, G., 2021. Mortars and plasters—how to characterise hydraulic mortars. *Archaeological and Anthropological Sciences* 13 (9), 1–22. https://doi.org/10.1007/s12520-021-01404-2.

Ashkenazi, D., Fantalkin, A., 2019. Archaeometallurgical and archaeological investigation of Hellenistic metal objects from Ashdod-Yam (Israel). *Archaeological and Anthropological Sciences* 11, 913–935. https://doi.org/10.1007/s12520-017-0579-1.

Ashkenazi, D., Shnabel, R., Lichtenberger, A., Tal, O., 2021. Chemical composition and microstructure analysis of plaster and pigments retrieved from a decorated house wall at Seleucid Tell Iẓṭabba (Nysa-Scythopolis, Beth She'an, Israel). *Mediterranean Archaeology and Archaeometry* 21 (3), 89–122. https://doi.org/10.5281/zenodo.5598239.

Asscher, Y., Ricci, G., Reato, M., Leviant, A., Peters, I., Neguer, J., Avrahami, M., Artioli, G., 2025. Implementation of red ochre in *Sinopia*: non-invasive characterization of the invisible frescos beneath Roman and Byzantine mosaics in Judea. *Journal of Archaeological Science* 175, 106146. https://doi.org/10.1016/j.jas.2024.106146.

Berna, F., Behar, A., Shahack-Gross, R., Berg, J., Boaretto, E., Gilboa, A., Sharon, I., Shalev, S., Shilstein, S., Yahalom-Mack, N., Zorn, J.R., 2007. Sediments exposed to high temperatures: reconstructing pyrotechnological processes in Late Bronze and Iron Age strata at Tel Dor (Israel). *Journal of Archaeological Science* 34 (3), 358–373. https://doi.org/10.1016/j.jas.2006.05.011.

Birney, K., 2017. Phoenician bathing in the Hellenistic East: Ashkelon and beyond. *Bulletin of the American Schools of Oriental Research* 378, 203–222.

Bochen, G., Labus, M., 2013. Study on physical and chemical properties of external lime–sand plasters of some historical buildings. *Construction and Building Materials* 45 (1), 11–19. http://dx.doi.org/10.1016/j.conbuildmat.2013.03.086.

Bonnie, R., Holmqvist, E., Kouki, P., Zissu, B., 2025. Plasters from Jewish ritual purification baths in Late Hellenistic–Early Roman Palestine: composition, production areas, and anthropogenic residues. *Heritage Science* 13 (1), 78. https://doi.org/10.1038/s40494-025-01594-1.

Cortea, I.M., Ghervase, L., Ratoiu, L., Țentea, O., Dinu, M., 2024. New insights into the materials and painting techniques of ancient wall paintings from the Roman province of Dacia: a minimally invasive multi-method approach. *Heritage* 7 (9), 5268–5294. https://doi.org/10.3390/heritage7090248.

David, P.A., 1985. Clio and the economics of QWERTY. *The American Economic Review* 75 (2), 332–337.

Dayet, L., 2021. Invasive and non-invasive analyses of ochre and iron-based pigment raw materials: a methodological perspective. *Minerals* 11 (2), 210. https://doi.org/10.3390/min11020210.

Ergenç, D., Fort, R., Varas-Muriel, M.J., Alvarez de Buergo, M., 2021. Mortars and plasters—how to characterize aerial mortars and plasters. *Archaeological and Anthropological Sciences* 13, 197. https://doi.org/10.1007/s12520-021-01398-x.

Fantalkin, A., Mazis, M., Schauer, Y., Ariel, D.T., Krispin, S., Tsuf, O., Eshel, T., Itkin, E., 2024. Hellenistic Ashdod-Yam in light of recent archaeological investigations. *Tel Aviv* 51 (2), 238–278. https://doi.org/10.1080/03344355.2024.2385149.

Friesem, D.E., Abadi, I., Shaham, D., Grosman, L., 2019. Lime plaster cover of the dead 12,000 years ago—new evidence for the origins of lime plaster technology. *Evolutionary Human Sciences* 1, e9.

Friesem, D.E., Anton, M., Waiman-Barak, P., Shahack-Gross, R., Nadel, D., 2020. Variability and complexity in calcite-based plaster production: a case study from a Pre-Pottery Neolithic B infant burial at Tel Roʻim West and its implications to mortuary practices in the southern Levant. *Journal of Archaeological Science* 113, 105048. https://doi.org/10.1016/j.jas.2019.105048.

Fischer, M., 2008. Yavneh-Yam, in: Stern, E. (Ed.), *The New Encyclopedia of Archaeological Excavations in the Holy Land* 5. Israel Exploration Society, Jerusalem, pp. 2073–2075.

Fischer, M., Fantalkin, A., Taxel, I., Bouzaglou, L., Tal, O., 2023. Clay boat models from Yavneh-Yam: towards an understanding of their chronology, function and use. *Journal of Eastern Mediterranean Archaeology and Heritage Studies* 11 (2–3), 337–353. https://doi.org/10.5325/jeasmedarcherstu.11.2-3.0337.

Fischer, M., Roll, I., Tal, O., 2008. Persian and Hellenistic remains at Tel Ya'oz. *Tel Aviv* 3 5(1), 123–163. https://doi.org/10.1179/tav.2008.2008.1.123.

Foerster, G., 1995. *Masada: The Yigael Yadin Excavations 1963–1965: Final Reports. Art and Architecture*. Israel Exploration Society, Jerusalem.

Goshen, N., Yasur-Landau, A., Cline, E.H., Shahack-Gross, R., 2017. Palatial architecture under the microscope: production, maintenance, and spatiotemporal changes gleaned from plastered surfaces at a Canaanite palace complex, Tel Kabri, Israel. *Journal of Archaeological Science: Reports* 11, 189–199. https://doi.org/10.1016/j.jasrep.2016.11.039.

Grono, E., Edrey, M., Morstadt, B., Bampton, P., Zuckerman-Cooper, R., Paz, G.B., Langgut, D., Friesem, D.E., 2024. Identifying construction technologies and environmental connections at the Iron Age IIA settlement of Kh. es-Suwweida, Israel: a microarchaeological study. *Journal of Archaeological Science: Reports* 60, 104850. https://doi.org/10.1016/j.jasrep.2024.104850.

Guglielmi, V., Comite, V., Andreoli, M., Demartin, F., Lombardi, C.A., Fermo, P., 2020. Pigments on Roman wall painting and stucco fragments from the Monte d'Oro Area (Rome): a multi-technique approach. *Applied Sciences* 10 (20), 7121. https://doi.org/10.3390/app10207121.

Guirdzhiiska, D., Zlateva, B., Glavcheva, Z., 2017. Polished decorative fields in Thracian fresco tombs from the Hellenistic period—archaeometrical research. *STAR: Science and Technology of Archaeological Research* 3 (2), 428–436. https://doi.org/10.1080/20548923.2017.1396723.

Humbert, J.-B., 2012. La maisons hellénistique aux murs peints, in: Humbert, J.-B. (Ed.), *Mission archéologique de Gaza: coopération franco-palestinienne 1995–2005, Jerusalem*. Ecole Biblique et Archéologique de Jérusalem, Jerusalem, pp. 226–239.

Jackson, H., 2016. Stucco fragments from the acropolis palace, in: Clarke, G., Jackson, H.M., Nixon, C.E.V., Tidmarsh, J., Wesselingh, K., Cougle, L. (Eds.), *Jebel Khalid on the Euphrates V: Report on Excavations 2000–2010* (Mediterranean Archaeology Supplement 10). MEDITARCH Publications; Sydney University Press, Sydney, pp. 259–268.

Kidd, B., 2018. Decorative wall plaster, in: Berlin A.M., Herbert, S.C. (Eds.), *Tel Anafa* II, iii: *Decorative Wall Plaster, Objects of Personal Adornment and Glass Counters, Tools for Textile Manufacture and Miscellaneous Bone, Terracotta and Stone Figurines, Pre-Persian Pottery, Attic Pottery, and Medieval Pottery*. Kelsey Museum of Archaeology, Ann Arbor, pp. 5–78.

Kingery, W.D., Vandiver, P.B., Prickett, M., 1988. The beginnings of pyrotechnology, part II: production and use of lime and gypsum plaster in the Pre-Pottery Neolithic Near East. *Journal of Field Archaeology* 15 (2), 19–243. https://doi.org/10.1179/009346988791974501.

Klempan, B., Helwig, K., Colivicchi, F., 2017. Examination and analysis of Etruscan wall paintings at Caere, Italy. *Archaeometry* 59 (6), 1082–1094. https://doi.org/10.1111/arcm.12304.

Laidlaw, A., 1985. *The First Style in Pompeii: Painting and Architecture*. Bretschneider, Rome.

Lave, J., Wenger, E., 1991. *Situated Learning: Legitimate Peripheral Participation*. Cambridge University Press, Cambridge.

Ling, R., 1991. *Roman Painting.* Cambridge University Press, Cambridge.

Lorenzon, M., 2023. Earthen architecture as a community of practice: a case study of Neolithic earthen production in the eastern Mediterranean. *Cambridge Archaeological Journal* 33 (4), 601–618. https://doi.org/10.1017/S0959774323000033.

Maeir, A.M., 2020. The Beth-Shean Valley: geographical and environmental background, in: Mazar, A., Panitz-Cohen, N. (Eds.), *Tel Reḥov: A Bronze and Iron Age City in the Beth-Shean Valley* I: *Introductions, Synthesis and Excavations on the Upper Mound* (Qedem 59). Hebrew University of Jerusalem, Jerusalem, pp. 1–11.

Marketou, A.K., Kouzeli, K., Facorellis, Y., 2019. Colourful earth: iron-containing pigments from the Hellenistic pigment production site of the ancient Agora of Kos (Greece). *Journal of Archaeological Science: Reports* 26, 101843. https://doi.org/10.1016/j.jasrep.2019.05.008.

Mastrotheodoros, G.P., Beltsios, K.G., 2022. Pigments—iron-based red, yellow, and brown ochres. *Archaeological and Anthropological Sciences* 14 (35), 2–25. https://doi.org/10.1007/s12520-021-01482-2.

Mateos, L.D., Esquivel, D., Cosano, D., Jiménez-Sanchidrián, C., Ruiz, J.R., 2018. Micro-Raman analysis of mortars and wall paintings in the Roman villa of Fuente Alamo (Puente Genil, Spain) and identification of the application technique. *Sensors and Actuators A: Physical* 281, 15–23. https://doi.org/10.1016/j.sna.2018.08.038.

Medeghini, L., Calzolari, L., Botticelli, M., Di Fazio, M., De Vito, C., Pettiti, I., Bardelli, F., Mignardi, S., 2024. The secret of ancient Roman hydraulic mortar: the lesson learnt from the past for future cements. *Cement and Concrete Composites* 148, 105484. https://doi.org/10.1016/j.cemconcomp.2024.105484.

Miriello, D., Bloise, A., Crisci, G.M., De Luca, R., De Nigris, B., Martellone, A., Osanna, M., Pace, R., Pecci, A., Ruggieri, N., 2018. Non-destructive multi-analytical approach to study the pigments of wall painting fragments reused in mortars from the archaeological site of Pompeii (Italy). *Minerals* 8 (4), 134. https://doi.org/10.3390/min8040134.

Moropoulou, A., Bakolas, A., Bisbikou, K., 2000. Investigation of the technology of historic mortars. *Journal of Cultural Heritage* 1 (1), 45–58. https://doi.org/10.1016/S1296-2074(99)00118-1.

Pizzo, P., Válek, J., Kozlovcev, P., Frankeová, D., Viani, A., 2024. Plasters and mortars from the theatre in Nea Paphos (Cyprus): a multidisciplinary study. *Journal of Archaeological Science: Reports* 57, 104595. https://doi.org/10.1016/j.jasrep.2024.104595.

Poduska, K.M., Regev, L., Berna, F., Mintz, E., Milevski, I., Khalaily, H., Weiner, S., Boaretto, E., 2012. Plaster characterization at the PPNB site of Yiftahel (Israel) including the use of 14C: implications for plaster production, preservation, and dating. *Radiocarbon* 54 (3–4), 887–896. https://doi.org/10.1017/S0033822200047536.

Radpour, R., Fischer, C., Kakoulli, I., 2019. New insight into Hellenistic and Roman Cypriot wall paintings: an exploration of artists' materials, production technology, and technical style. *Arts* 8 (2), 74. https://doi.org/10.3390/arts8020074.

Ravi, R., Thirumalini, S., Taher, N., 2018. Analysis of ancient lime plasters—reason behind longevity of the Monument Charminar, India a study. *Journal of Building Engineering* 20, 30–41. https://doi.org/10.1016/j.jobe.2018.04.010.

Regev, L., Poduska, K.M., Addadi, L., Weiner, S., Boaretto, E., 2010. Distinguishing between calcites formed by different mechanisms using infrared spectrometry: archaeological applications. *Journal of Archaeological Science* 37 (12), 3022–3029. https://doi.org/10.1016/j.jas.2010.06.027.

Roux, V., 2015. Standardization of ceramic assemblages: transmission mechanisms and diffusion of morpho-functional traits across social boundaries. *Journal of Anthropological Archaeology* 40, 1–9. https://doi.org/10.1016/j.jaa.2015.04.004.

Rozenberg, S., 2008. *Hasmonean and Herodian Palaces at Jericho, Final Reports of the 1973–1987 Excavations* IV: *The Decoration of Herod's Third Palace at Jericho.* Israel Exploration Society and the Hebrew University of Jerusalem, Jerusalem.

Rozenberg, S., 2019. Stuccowork in the ancient Land of Israel. *Syria* 96, 183–200. https://doi.org/10.4000/12cj9.

Sandler, A., Taitel-Goldman, N., Ezersky, V., 2023. Sources and formation of iron minerals in eastern Mediterranean coastal sandy soils—a HRTEM and clay mineral study. *Catena* 220, 106644. https://doi.org/10.1016/j.catena.2022.106644.

Sharma, A., Singh, M.R., 2021. A review on historical earth pigments used in India’s wall paintings. *Heritage* 4 (3), 1970–1994. https://doi.org/10.3390/heritage4030112.

Singh, M., Kumar, S.V., Sabale, P.D., 2019. Chemical and mineralogical investigations of lime plasters of medieval structures of Hampi, India. *International Journal of Architectural Heritage* 13 (5), 725–741. https://doi.org/10.1080/15583058.2018.1469175.

Steidl, C., 2020. The dynamics of belonging: comparative community formation in the East and West Mediterranean. *Journal of Mediterranean Archaeology* 33, 79–101. https://doi.org/10.1558/jma.42348.

Tal, O., Reshef, N., 2017. Hellenistic stratigraphy and architecture, in: Greenberg, R., Tal, O., Da‘adli, T. *Bet Yeraḥ* III: *Hellenistic Philoteria and Islamic al-Ṣinnabra* (IAA Reports 61). Israel Antiquities Authority, Jerusalem, pp. 13–58.

Tarassova, E., Tarassov, M., 2023. Comparative characteristics of ancient red pigments used to decorate Thracian sacred sites (4th–3rd centuries BC). *Review of the Bulgarian Geological Society* 84 (2), 63–67. https://doi.org/10.52215/rev.bgs.2023.84.2.63.

Teklay, M., Thole, J.T., Ndumbu, N., Vries, J., Mezger, K., 2023. Mineralogical and chemical characterization of ochres used by the Himba and Nama people of Namibia. *Journal of Archaeological Science: Reports* 47, 103690. https://doi.org/10.1016/j.jasrep.2022.103690.

Vázquez de Ágredos-Pascual, M.L., Zapata-Meza, M., Sanz-Rincón, R., Garza DíazBarriga, A., Expósito De Vicente, C., Rojo-Iranzo, L., Herreras Sala, S., 2019. Physicochemical and cultural study of coloring materials from 1st c. AD Magdala, Lower Galilee. *Mediterranean Archaeology and Archaeometry* 19 (3), 173–188. https://doi.org/10.5281/zenodo.3583077.

Wendrich, W. (Ed.), 2012. *Archaeology and Apprenticeship: Body Knowledge, Identity, and Communities of Practice*. University of Arizona Press, Tucson.

Appendix A: Location maps of stucco fragment samples from Ashdod-Yam, Yavneh-Yam, and Tel Ya‘oz

This appendix presents plans of the sites of Ashdod-Yam (Fig. A1), Yavneh-Yam (Fig. A2), and Tel Ya‘oz (Fig. A3), marked with the findspots of stucco fragments analyzed in the present study.

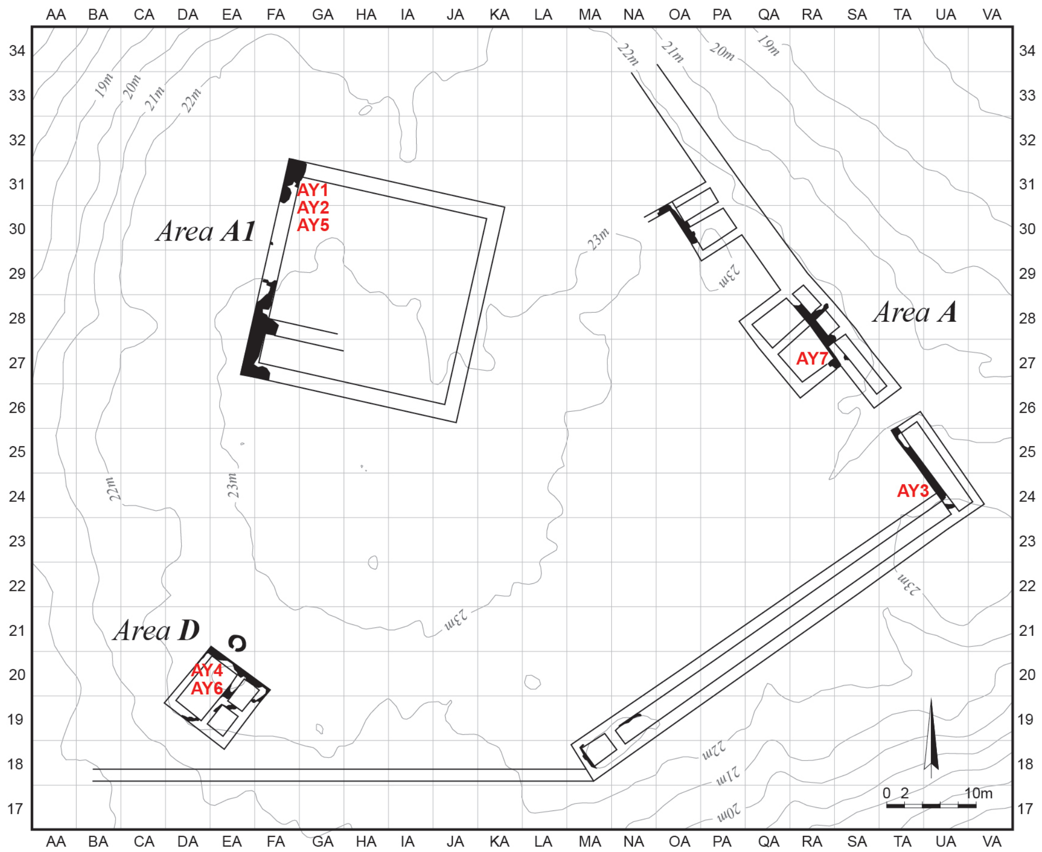

Figure A1. Plan of Ashdod-Yam Areas A, A1, and D, with indication of sample (AY1–AY7) provenance.

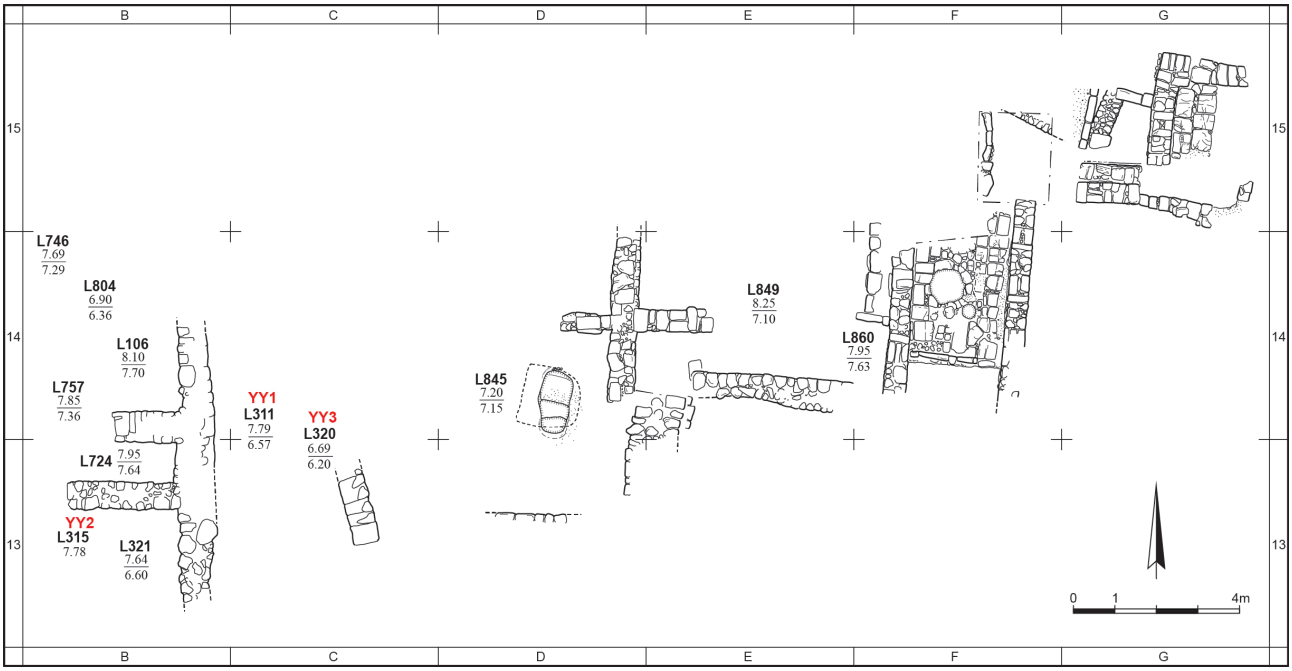

Figure A2. Plan of Yavneh-Yam Area A, with indication of sample (YY1–YY3) provenance.

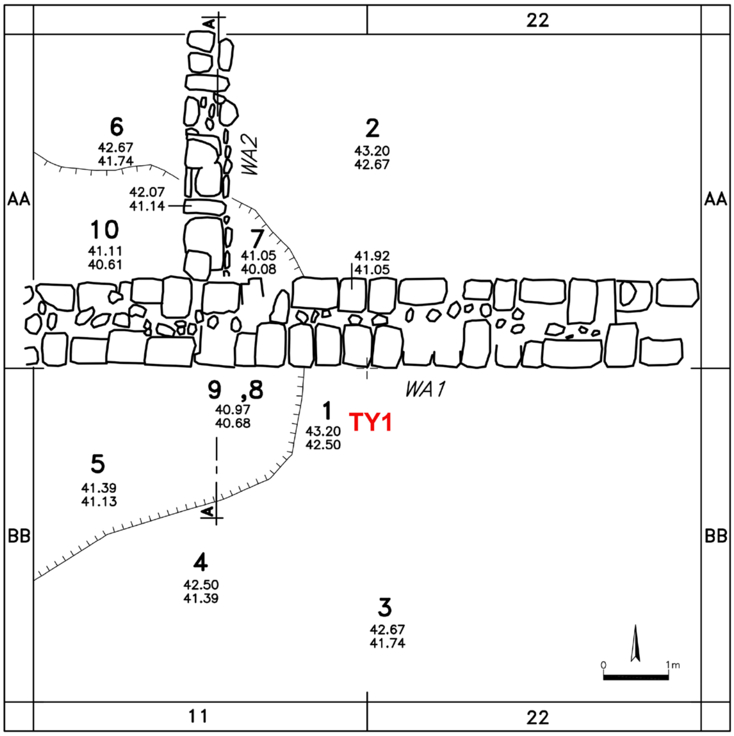

Figure A3. Plan of Tel Ya'oz Area A, with indication of sample (TY1) provenance.

Appendix B: Description of samples, excavation contexts, and applied analytical methods

Table B1. Provenance, description, and examination methods of stucco samples from Ashdod-Yam (AY), Yavneh-Yam (YY), and Tel Ya'oz (TY).

<table>
<tr><th rowspan="2">Sample no.</th><th rowspan="2">Location</th><th rowspan="2">Description</th><th colspan="4">Examination method</th></tr>
<tr><th>VT</th><th>SEM-EDS</th><th>FTIR</th><th>XRD</th></tr>
<tr><td>AY1</td><td>Ashdod-Yam Area A1, Locus 230, Basket 1185</td><td>Red pigment with underlying plaster</td><td>+</td><td>+</td><td>–</td><td>+</td></tr>
<tr><td>AY2</td><td>Ashdod-Yam Area A1, Locus 231, Basket 1255</td><td>Red pigment with underlying plaster</td><td>+</td><td>+</td><td>+</td><td>–</td></tr>
<tr><td>AY3</td><td>Ashdod-Yam Area A, Locus 136, Basket 10174</td><td>Plaster covered with red pigment</td><td>+</td><td>+</td><td>–</td><td>–</td></tr>
<tr><td>AY4</td><td>Ashdod-Yam Area D, Locus 5071, Basket 50187</td><td>Two layers of plaster covered with red paint</td><td>+</td><td>+</td><td>–</td><td>–</td></tr>
<tr><td>AY5</td><td>Ashdod-Yam Area A1, Locus 200, Basket 1088</td><td>Black pigment with underlying plaster</td><td>+</td><td>+</td><td>+</td><td>–</td></tr>
<tr><td>AY6</td><td>Ashdod-Yam Area D, Locus 5095, Basket 50223</td><td>Plaster</td><td>+</td><td>+</td><td>+</td><td>–</td></tr>
<tr><td>AY7</td><td>Ashdod-Yam Area A, Locus 155, Basket 10253</td><td>Plaster layer over composite mortar base</td><td>+</td><td>–</td><td>+</td><td>–</td></tr>
<tr><td>YY1</td><td>Yavneh-Yam Area A, Locus 311, Basket 3019</td><td>Two layers of white plaster with painted red stripe between them</td><td>+</td><td>+</td><td>+</td><td>–</td></tr>
<tr><td>YY2</td><td>Yavneh-Yam Area A, Locus 315, Basket 3030</td><td>Red pigment with underlying plaster</td><td>+</td><td>+</td><td>+</td><td>–</td></tr>
<tr><td>YY3</td><td>Yavneh-Yam Area A, Locus 320, Basket 3073</td><td>Red pigment with underlying plaster</td><td>+</td><td>+</td><td>+</td><td>+</td></tr>
<tr><td>TY1</td><td>Tel Ya'oz Area A, Locus 1, Item 6 (Sample 1011)</td><td>Red pigment with underlying plaster</td><td>+</td><td>+</td><td>+</td><td>–</td></tr>
<tr><td>TY2.1</td><td rowspan="2">Tel Ya'oz Area A, Locus 1, Item 6 (Sample 1023)</td><td rowspan="2">Red pigment with underlying plaster</td><td rowspan="2">+</td><td>+</td><td>+</td><td>–</td></tr>
<tr><td>TY2.2</td><td>–</td><td>+</td><td>–</td></tr>
<tr><td>TY3</td><td>Tel Ya'oz Area A, Locus 1, Item 6 (Sample 1026)</td><td>Red pigment with underlying plaster</td><td>+</td><td>+</td><td>+</td><td>–</td></tr>
<tr><td>TY4</td><td>Tel Ya'oz Area A, Locus 1, Item 6 (Sample 1110)</td><td>Red pigment with underlying plaster</td><td>+</td><td>–</td><td>+</td><td>–</td></tr>
<tr><td>TY5.1</td><td rowspan="5">Tel Ya'oz Area A, Locus 1, Item 6 (Sample 1034)</td><td rowspan="5">Red pigment with underlying plaster</td><td rowspan="5">+</td><td rowspan="5">–</td><td rowspan="5">–</td><td rowspan="5">–</td></tr>
<tr><td>TY5.2</td></tr>
<tr><td>TY5.3</td></tr>
<tr><td>TY5.4</td></tr>
<tr><td>TY5.5</td></tr>
<tr><td>TY6.1</td><td rowspan="6">Tel Ya'oz Area A, Locus 1, Item 6 (Sample 1064)</td><td rowspan="6">Red pigment with underlying plaster</td><td rowspan="6">+</td><td>+</td><td rowspan="6">–</td><td>+</td></tr>
<tr><td>TY6.2</td><td rowspan="5">–</td><td rowspan="5">–</td></tr>
<tr><td>TY6.3</td></tr>
<tr><td>TY6.4</td></tr>
<tr><td>TY6.5</td></tr>
<tr><td>TY6.6</td></tr>
</table>

Appendix C: SEM-EDS results of stucco samples from Ashdod-Yam, Yavneh-Yam, and Tel Ya'oz

To complement the mineralogical and macroscopic examinations, selected plaster and pigment samples were analyzed using SEM-EDS. Since this method provides semi-quantitative results that are influenced by factors such as surface roughness and sample heterogeneity, obtained chemical data are presented here for comparative and interpretative purposes. All detailed compositional results are compiled in this appendix rather than in the main text.

Table C1. SEM-EDS results of the Ashdod-Yam paint and plaster samples; SA represents the scanned area.

Sample no. and description	Composition weight percentage (wt.%)									
	CaO	SiO_2	Fe_2O_3	Al_2O_3	MgO	K_2O	TiO_2	Sb_2O_5	SO_3	P_2O_5
AY1, plaster with areas of red pigment (PS), AS1: 800 µm × 800 µm	55.7	21.4	9.0	10.3	1.8	1.8	–	–	–	–
AY1, red pigment (PS, Fig. 4b), upper part of sample, SA: 150 µm × 150 µm	60.6	8.0	26.4	5.0	–	–	–	–	–	–
AY2, plaster (TCS), AS2: 300 µm × 300 µm	89.9	2.0	1.3	1.0	1.3	–	–	4.5	–	–
AY3, red pigment (PS, Fig. 4a), SA 1: 250 µm × 250 µm	42.9	20.0	22.4	10.1	1.7	1.7	1.2	–	–	–
AY3, red pigment, (PS, Fig. 4a), SA 2: 30 µm × 30 µm	26.1	5.9	56.9	9.5	–	–	0.8	–	0.8	–
AY3, red pigment (PS), upper part of sample, SA 3: 300 µm × 300 µm	25.0	35.4	15.8	17.6	2.5	2.5	1.2	–	–	–
AY3, red pigment (PS), upper part of sample, SA 4: 300 µm × 300 µm	67.1	8.4	17.3	5.6	0.8	0.8	–	–	–	–
AY4, red pigment, lower layer (PS, Fig. 3c), SA 1: 150 µm × 150 µm	45.5	15.5	27.3	7.9	1.8	1.1	0.9	–	–	–
AY4, red pigment, lower layer (PS, Fig. 3d), SA 2: 50 µm × 50 µm	46.4	8.8	33.6	8.3	1.2	–	1.2	–	0.5	–
AY4, red pigment, upper layer (PS), left side of sample, SA 1: 500 µm × 500 µm	81.0	3.6	11.5	2.9	1.0	–	–	–	–	–
AY4, red pigment, upper layer (PS), SA 2: 150 µm × 150 µm	56.5	4.2	37.2	2.1	–	–	–	–	–	–
AY4, red pigment, upper layer (PS), SA 3: 40 µm × 40 µm	8.8	2.6	78.5	9.4	–	–	–	–	0.7	–
AY5, black pigment, central part of sample (PS, Fig. 4c), SA 1: 800 µm × 800 µm	69.4	14.2	2.3	9.3	4.0	0.8	–	–	–	–
AY5, black pigment, central part of sample (PS, Fig. 4d), SA 2: 500 µm × 500 µm	71.2	12.6	2.1	10.6	2.6	–	–	–	–	0.9
AY5, black pigment, central part of sample (PS), SA 3: 500 µm × 500 µm	78.1	11.1	1.9	6.4	2.5	–	–	–	–	–
AY5, plaster (TS), SA 1: 500 µm × 500 µm	71.1	14.6	1.8	8.5	4.0	–	–	–	–	–
AY5, plaster (TS), SA 2: 500 µm × 500 µm	60.1	24.0	3.6	9.0	3.3	–	–	–	–	–
AY6, bright plaster with particles (TS), SA 2: 60 µm × 60 µm	95.4	2.5	–	2.1	–	–	–	–	–	–

Table C2. SEM-EDS results of the Yavneh-Yam paint and plaster samples; SA represents the scanned area.

Sample no. and description	Composition weight percentage (wt.%)									
	CaO	SiO_2	Fe_2O_3	Al_2O_3	MgO	K_2O	TiO_2	Sb_2O_5	SO_3	P_2O_5
YY1, upper plaster, (TS), SA 1: 800 µm × 800 µm	64.1	35.9	–	–	–	–	–	–	–	–
YY1, upper plaster (TS), SA 2: 500 µm × 500 µm	92.8	4.9	2.3	–	–	–	–	–	–	–
YY1, plaster with red pigment particles (PS, Fig. 7a), SA 1: 500 µm × 500 µm	79.8	11.2	3.5	3.2	1.3	–	–	–	–	1.0
YY1, red pigment (PS, Fig. 7b), SA 2: 150 µm × 150 µm	41.6	40.8	6.6	7.2	1.9	1.9	–	–	–	–
YY1, red pigment (PS), SA 3: 250 µm × 250 µm	82.7	9.9	4.5	2.9	–	–	–	–	–	–
YY2, red pigment (PS, Fig. 7c-d), SA 1: 800 µm × 800 µm	58.4	20.6	9.6	6.6	2.1	1.0	–	–	1.7	–
YY2, red pigment (PS, Fig. 7e), SA 2: 250 µm × 250 µm	70.3	12.0	9.2	4.7	1.7	–	–	–	1.2	0.9
YY3, red pigment (PS, Fig. 7f), SA 1: 250 µm × 250 µm	74.9	2.7	21.1	1.3	–	–	–	–	–	–

Table C3. SEM-EDS results of the Tel Yaʻoz paint and plaster samples; SA represents the scanned area.

Sample description	Composition weight percentage (wt.%)									
	CaO	SiO_2	Fe_2O_3	Al_2O_3	MgO	K_2O	TiO_2	As_2O_5	SO_3	P_2O_5
TY1, plaster with red pigment particles (PS, Fig. 11a), SA 1: 800 µm × 800 µm	58.0	24.3	12.2	5.5	–	–	–	–	–	–
TY1, red pigment (PS, Fig. 11d), SA 2: 60 µm × 60 µm	36.5	6.8	53.7	3.0	–	–	–	–	–	–
TY1, red pigment (PS), SA 3: 30 µm × 30 µm	8.6	4.5	82.1	1.9	–	–	–	2.2	0.7	–
TY2.1, plaster with red pigment particles (PS, Fig. 13b), SA 1: 150 µm × 150 µm	37.0	44.2	6.3	9.9	1.3	1.3	–	–	–	–
TY2.1, red pigment (PS), SA 2: 80 µm × 80 µm	40.8	26.5	16.1	13.4	1.4	1.8	–	–	–	–
TY2.1, red pigment (PS), SA 3: 80 µm × 80 µm	30.0	33.1	16.0	13.1	1.4	2.5	3.9	–	–	–
TY3, red pigment (PS, Fig. 14b), SA 1: 600 µm × 600 µm	28.8	7.3	59.9	3.4	–	–	0.6	–	–	–
TY3, red pigment (PS, Fig. 14c-d), SA 2: 80 µm × 80 µm	7.4	5.4	80.9	3.0	–	0.7	–	2.6	–	–
TY6.1, red pigment (PS, Fig. 14c-d), SA 1: 80 µm × 80 µm	25.6	13.8	58.8	1.8	–	–	–	–	–	–

Appendix D: FTIR results of the samples from Ashdod-Yam, Yavneh-Yam, Tel Ya'oz, and Tell Iẓṭabba

Calcite atomic order was assessed and interpreted using grinding curves, following the approach of Regev et al. (2010), which enables distinguishing between pyrogenic lime plaster and geogenic carbonate materials, on the basis of the degree of atomic disorder in the calcite structure (Figs. D1–D4).

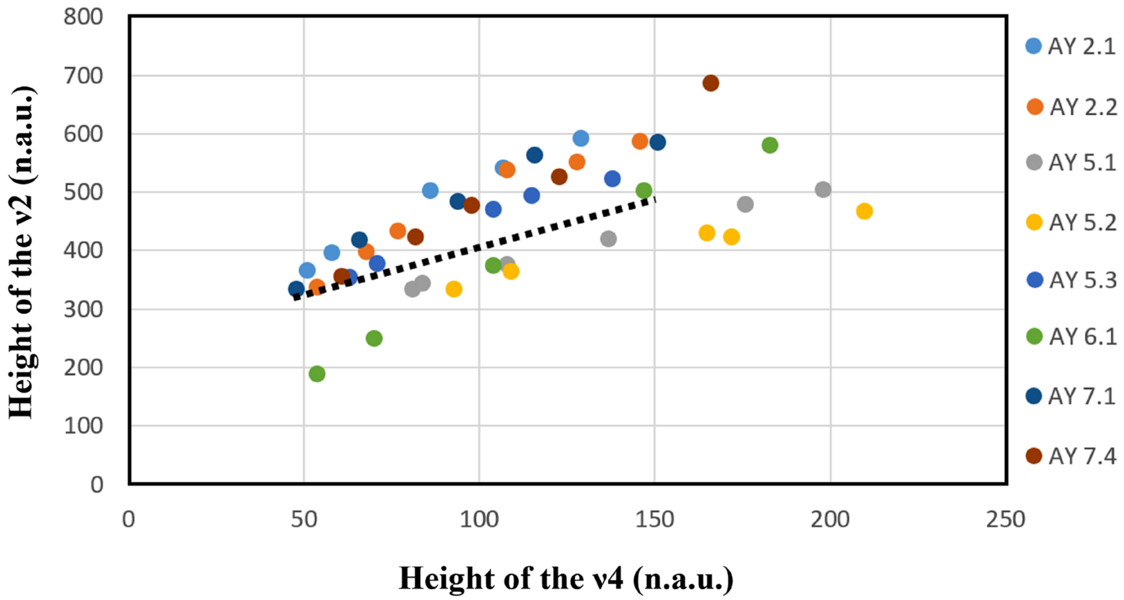

Fig. D1. FTIR grinding curve of calcite illustrating the relationship between the v absorption band height and the degree of crystallinity (atomic order) in the samples from Ashdod-Yam.

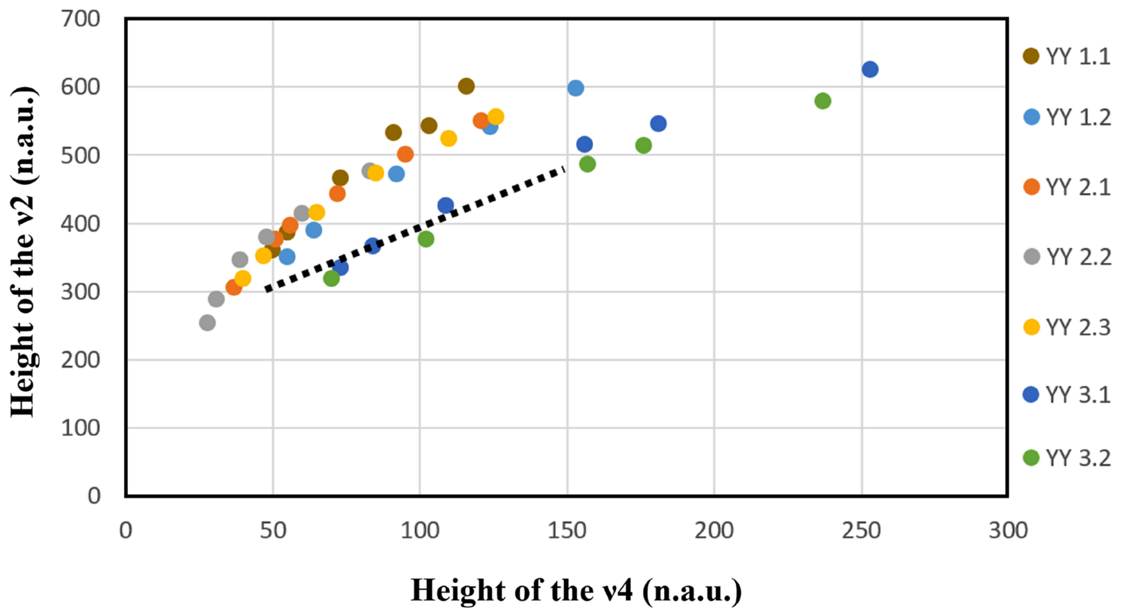

Fig. D2. FTIR grinding curve of calcite illustrating the relationship between the v absorption band height and the degree of crystallinity (atomic order) in the samples from Yavneh-Yam.

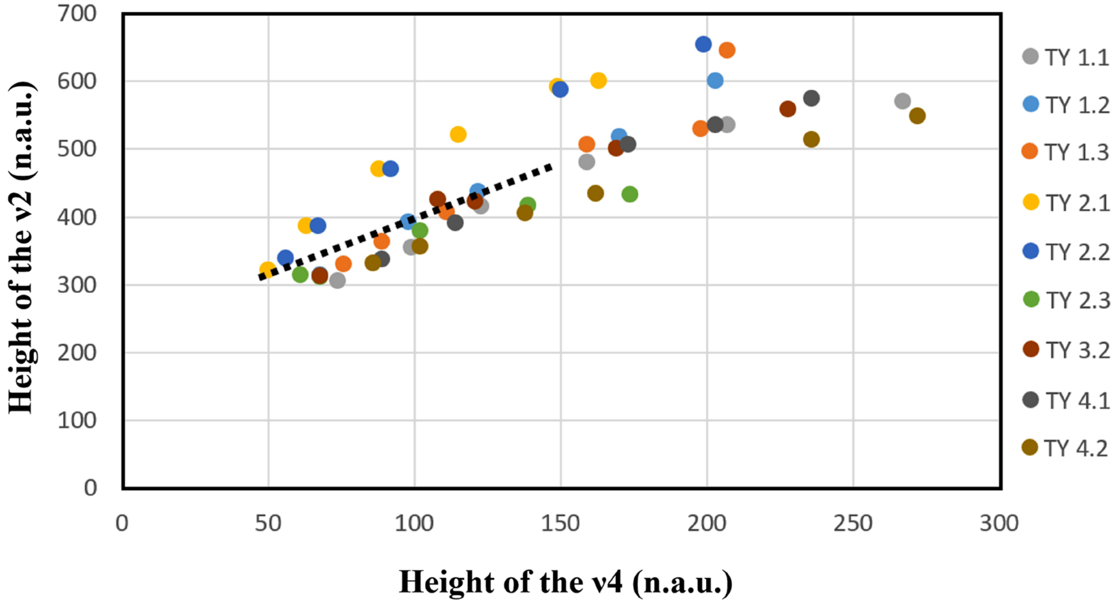

Fig. D3. FTIR grinding curve of calcite illustrating the relationship between the v absorption band height and the degree of crystallinity (atomic order) in the samples from Tel Ya'oz.

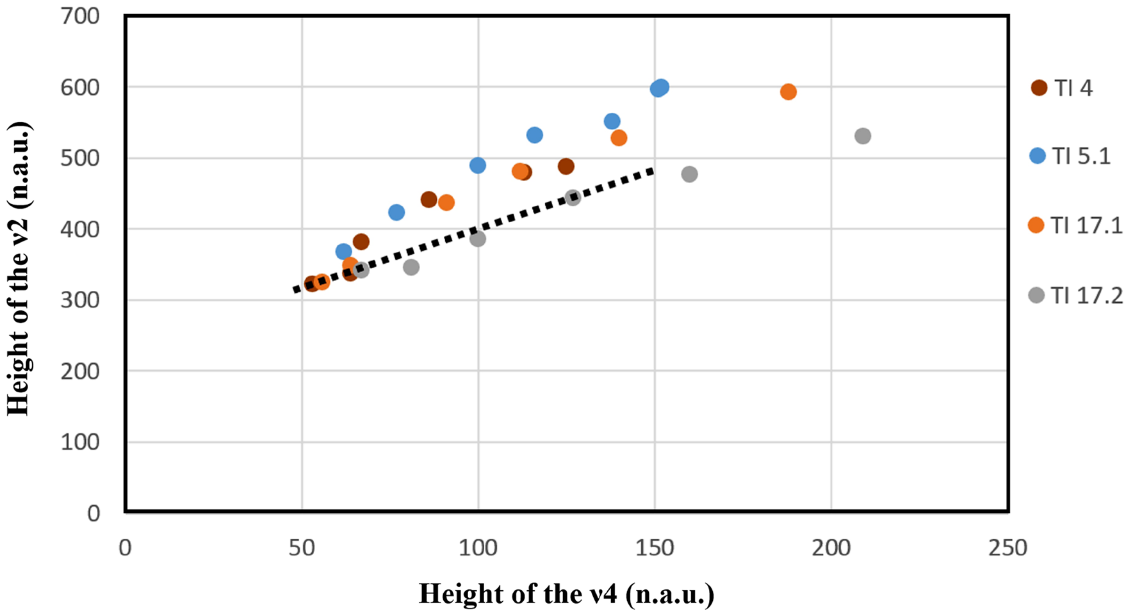

Fig. D4. FTIR grinding curve of calcite illustrating the relationship between the v absorption band height and the degree of crystallinity (atomic order) in the samples from Tell Iẓṭabba.

References

Regev, L., Poduska, K.M., Addadi, L., Weiner, S., Boaretto, E., 2010. Distinguishing between calcites formed by different mechanisms using infrared spectrometry: archaeological applications. *Journal of Archaeological Science* 37 (12), 3022–3029. https://doi.org/10.1016/j.jas.2010.06.027.

Appendix E: Archaeological background and FTIR results of the Tell Iẓṭabba samples

Archaeology of Tell Iẓṭabba

Tell Iẓṭabba (Nysa-Scythopolis), located in the Beth She'an Valley, has been investigated by a joint German-Israeli team since 2019, aiming to achieve a systematic understanding of the settlement history and economy of the Seleucid city (Ebeling et al., 2020; 2021; Edrey et al., 2023). Nysa-Scythopolis was one of several Graeco-Roman cities supported by the Hellenistic dynasties—first the Ptolemies, and later the Seleucids—that were later known as the Decapolis (Tal, 2011; Lichtenberger, 2020). A major formative phase of this group of cities occurred during the time of Antiochos IV, who founded Nysa-Scythopolis in the 160s BCE (Lichtenberger, 2008). The city was destroyed by John Hyrcanus I in the spring of 107 BCE (Lichtenberger et al., 2022).

Plaster and stucco fragments retrieved from a wall (Wall 307) of a domestic structure in Area C (Ebeling et al., 2020, pp. 184–187) were analyzed by Ashkenazi et al. (2021) as part of a study focusing mainly on pigment characterization, utilizing multiple methods, including visual testing (VT) and XRF, SEM-EDS, and XRD analyses. Results were combined with archaeological and geographical data. White-hued plaster from Tell Iẓṭabba was found to consist of calcite mixed with aggregates. SEM-EDS results showed that the fine plaster contained slightly more Ca and less Si compared to the coarse plaster, the latter displaying a higher abundance of sand particles. Red- and yellow-painted decorations on the Tell Iẓṭabba fragments contained red and yellow ochre pigments, respectively. Brown-paint was produced using a mixture of red ochre, yellow ochre, magnetite, and carbon black-based pigments. Black paint contained carbon black-based pigment. All pigments were mixed with fine plaster powder. Both plaster and pigments were likely produced and supplied regionally, and perhaps even locally (Ashkenazi et al., 2021).

FTIR results of the Tell Iẓṭabba samples

Mineralogical analysis was conducted using FTIR spectroscopy. Selected painted plaster samples from the site (n = 3: TI4, TI5, TI17, Table E1) were subdivided in the lab (n = 6: TI4, TI5.1, TI5.2, TI5.3, TI17.1, TI17.2; Table E1) to identify different components within each sample. Results indicate that all plasters and pigments include calcite with high atomic disorder, associated with pyrogenic formation of lime (Table E1). The highly disordered lime structure indicates good quality and standardization. The degree of calcite atomic order for the Tell Iẓṭabba samples was assessed using FTIR grinding curves following Regev et al. (2010) (see Appendix D, Fig. D4).

Table E1. FTIR results of the Tel Iẓṭabba (TI) samples. Calcite atomic order was assessed using FTIR grinding curves following Regev et al. (2010). Clay alteration due to exposure to elevated temperatures follows Berna et al. (2007). Ca = calcite; Cl = clay; (un) = unaltered; Q = quartz; G = gypsum; B = basalt

Sample no.	Location/sample type	Description	Major minerals	Calcite order
TI4	Tell Iẓṭabba, Wall 307, Area C, plaster	Homogeneous plaster with a few black, white, and yellow medium sand-sized inclusions	G>Ca	Disordered
TI5.1	Tell Iẓṭabba, Wall 307, Area C, red pigment with underlying plaster	Smooth red pigmented surface	Ca>Cl(un)>>Q	Disordered
TI5.2		White plaster	Ca>>>>Cl	
TI5.3		Coarse brown-black inclusions in plaster	B>>Ca	
TI17.1	Tell Iẓṭabba, Wall 307, Area C, plaster	Smoothed white plaster surface with coarse sand-sized brown-black inclusions	Ca>>>>Cl	Disordered
TI17.2		Beige sediment under plaster surface	Ca>>Cl(un)	Ordered/borderline

References

Ashkenazi, D., Shnabel, R., Lichtenberger, A., Tal, O., 2021. Chemical composition and microstructure analysis of plaster and pigments retrieved from a decorated house wall at Seleucid Tell Iẓṭabba (Nysa-Scythopolis, Beth She’an, Israel). *Mediterranean Archaeology and Archaeometry* 21 (3), 89–122.

Ebeling, P., Edrey, M., Harpak, T., Lichtenberger, A., Tal, O., 2020. Field report on the 2019 German-Israeli *Tell Iẓṭabbā* Excavation Project (Beth She’an), Israel. *Zeitschrift des Deutschen Palästina-Vereins* 136 (2), 176–190. https://www.jstor.org/stable/45381828 (accessed November 23, 2025)

Ebeling, P., Edrey, M., Harpak, T., Lichtenberger, A., Tal, O., 2021. Field report on the 2020 German-Israeli *Tell Iẓṭabbā* Excavation Project (Beth She’an), Israel. *Zeitschrift des Deutschen Palästina-Vereins* 137 (1), 60–74. https://www.jstor.org/stable/45389305 (accessed November 23, 2025).

Edrey, M., Ebeling, P., Harpak, T., Lichtenberger, A., Tal, O., 2023. Field report on the 2023 German-Israeli *Tell Iẓṭabbā* Excavation Project (Beth She’an), Israel. *Zeitschrift des Deutschen Palästina-Vereins* 139 (2), 218–233.

Lichtenberger, A., 2008. Artemis and Zeus Olympios in Roman Gerasa and Seleucid religious policy, in: Kaizer, T. (Ed.), *The Variety of Local Religious Life in the Near East in the Hellenistic and Roman Periods*. Leiden and Boston, Brill, pp. 133–153.

Lichtenberger, A., 2020. Decapolis. *Brill Encyclopedia of Early Christianity Online*. Leiden, Brill. https://doi.org/10.1163/2589-7993_EECO_SIM_00000878.

Lichtenberger, A., Mienis, H., Orendi, O., Pines, M., Rittner, O., Tal, O., 2022. For everything there is a season: more than a year of destruction at Seleucid Tell Iẓṭabba (Israel). *Antiquity* 96 (389), 1316–1323. https://doi.org/10.15184/aqy.2022.92.

Tal, O., 2011. ‘Hellenistic Foundations’ in Palestine, in: Grabbe, L.I., Lipschits, O. (Eds.), *Judah between East and West: The Transition from Persian to Greek Rule (ca. 400–200 BCE)* (Library of Second Temple Studies 74). New York and London, T&T Clark, pp. 242–254.